Flexible operation of low-inertia power systems connected via high voltage direct current interconnectors

Flexible Operation of Low-Inertia Power Systems Connected via High Voltage Direct Current Interconnectors

Vincenzo Trovato[1], Andrea Mazza[2] and Gianfranco Chicco[2]

[1]Department of Electrical and Electronic Engineering, Imperial College London – United Kingdom
[2]Dipartimento Energia "Galileo Ferraris", Politecnico di Torino - Italy

Abstract

The replacement of conventional synchronous generators with converter-interfaced generation units calls for increased amounts of flexibility. This paper proposes a novel formulation of the security-constrained unit commitment (SCUC) model applied to a multi-area power systems connected via High Voltage Direct Current (HVDC) links. From a system perspective, this paper provides a critical analysis of the synergies and differences between the exploitation of thermostatic loads and HVDC links when providing different layers of flexibility to the system. The former operate within a *local* dimension, while the latter enable *cross-border* exchange of flexibility. Eight different ancillary services are modelled to tackle generation/load outages and uncertainty/variability in renewable energy output. The model is applied to the Great Britain network, which is connected to the Irish network and to the one in Continental Europe. Results suggest a critical review of the operation of future low-carbon HVDC-interconnected systems. Feasibility studies on the benefit for interconnection should no longer neglect considerations on local post-fault frequency dynamics in each area of the system. Then, fundamental changes to the mechanisms that price ancillary services become necessary in order to align these mechanisms with the technical needs of the system.

Keywords: Power system operation, inertial response, HVDC, flexibility, thermostatic loads, unit commitment

Nomenclature

Acronyms

AC	Alternating Current
CCGT	Combined Cycle Gas Turbine
CDF	Cumulative Distribution Function
CE	Continental Europe
CR	Contingency Reserve
ECDF	Empirical CDF
GB	Great Britain
HR	High Frequency Response
HVDC	High Voltage Direct Current
IR	Ireland
NI	Natural Inertia
OCGT	Open Cycle Gas Turbine
OR	Operating Reserve
PR	Primary Response
QP	Quadratic Programming
RES	Renewable Energy Sources
RoCoF	Rate of Change of Frequency
SCUC	Security-Constrained Unit Commitment
SR	Secondary Response
TCLs	Thermostatically Controlled Loads

System parameters

$\hat{F}_k$	Objective function of the SCUC for scenario k
F_{n_q}	ECDF relative to quantile n_q
h_{Γ_x}	Constant of inertia associated to Γ_x
K	Number of simulated scenarios
k	Index of scenario $k \in \{1, \dots, K\}$
N_q	Number of quantiles
n_q	Index of quantiles $n_q \in \{1, \dots, N_q\}$
N	Number of days
n	Index of days $n \in \{1, \dots, N\}$
Q_x	Nadir constraint function for generation outage in area x
$\underline{\mathcal{R}}_{n_q}$	Lower bound of wind in F_{n_q}
$\overline{\mathcal{R}}_{n_q}$	Upper bound of wind in F_{n_q}
T	Number of optimisation steps in a day
t	Index of time steps $t \in \{1, \dots, T\}$
t_{H_x}	Delivery time of HR in area x
t_{P_x}	Delivery time for PR in area x
t_ρ	Interval time for RoCoF condition
V	Annual vector of wind availability
$\vec{V}$	Sorted V in ascending order
v_{n_q}	Vector of element of V falling in quantile n_q
W_t	Requirement for OR at t
W_t^d	Requirement for downwards OR at t
x	Index of area e.g. $x \in \{\text{GB}, \text{IR}, \text{CE}\}$
Z_x	Nadir constraint function for load outage in area x
Γ_x	Maximum generation loss in area x
Δf_{nad}	Maximum frequency deviation at nadir
Δf_{qss}	Maximum quasi-steady state frequency deviation

Δf_ρ	Maximum frequency deviation for RoCoF
Δt	Duration of optimisation interval
Δt_a	Time duration of SR
Δt_b	Delivery time for CR
Δt_c	Additional time for CR
$\underline{\varepsilon}$	Probability level for OR (upwards)
$\overline{\varepsilon}$	Probability level for OR (downwards)
Λ_x	Maximum load outage in area x
$\lambda_{(\#),t}$	Lagrange multiplier of constraint (#) at t

Generation parameters

c_g^{lp}	production cost of g relative to $G_{g,t}$
c_g^{nl}	No-load cost of technology g
c_g^{ql}	production cost of g relative to ${G^2}_{g,t}$
c_g^{su}	Start-up cost of technology g
g	Index for generation technology
$\overline{G}_{g,t}$	maximum capacity of technology g at t
$\mathcal{G}$	Set of all generation technologies
$\mathcal{G}_x$	Set of generation technologies in area x
h_g	Constant of inertia of technology g
N_g^u	Number of equivalent units of technology g
t_g^d	Minimum down time for technology g
t_g^{sd}	Shut-down time for technology g
t_g^{su}	Start-up time for technology g
t_g^u	Minimum up time for technology g
γ_g	Minimum dispatch for technology g
μ_g	Ramp rate for response services of g
π_g	Headroom for response services for technology g
σ_g	Slope for response services for technology g

Load parameters

D_x	Load damping coefficient in area x
$E_{x,0}$	Steady-state TCL energy in area x
$\overline{E}_x$	Maximum TCL energy in area x
$\underline{E}_x$	Minimum TCL energy in area x
$L_{x,t}$	Inflexible load at time t in area x
$\widetilde{N}_x$	Number of TCLs in area x
$P_{x,0}$	Steady-state TCL power in area x
α_1-α_{10}	Numerical parameters for TCL constraints
$\overline{\theta}_x$	Maximum TCL power in area x
$\underline{\theta}_x$	Minimum TCL power in area x

Interconnectors parameters

c_t^{I}	GB-CE HVDC import/export cost at t
$\overline{I}_{CE}^{GB}$	Power rating of CE-GB interconnector
$\overline{I}_{GB}^{IR}$	Power rating of GB-IR interconnector

Decision variables

$C_{g,t}$	CR for technology g at time t
$C_{g,t}^d$	Downwards CR for technology g at t
$E_{x,t}$	TCL energy at the start of t in area x
$G_{g,t}$	Generation output of technology g at t
$H_{g,t}$	HR from generation g at time t
$\widetilde{H}_{x,t}$	HR from TCLs at time t in area x
I_t	GB-CE Interconnection power level at t
$O_{g,t}$	OR for technology g at t
$O_{g,t}^d$	Downwards OR for technology g at t
$P_{g,t}$	PR from generation g at time t
$\tilde{P}_{x,t}$	PR from TCL at time t in area x
$S_{g,t}$	SR from generation g at time t
$\tilde{S}_{x,t}$	SR from TCLs at time t in area x
$\zeta_{g,t}$	Capacity of g for standing reserve at t
$\theta_{x,t}$	TCL load at time t in area x
ξ_k	Set of all decision variables in scenario k
$\varphi_{g,t}$	On-line capacity of technology g at t
$\chi_{g,t}$	Capacity of technology g starting-up at t
$\psi_{g,t}$	Capacity of technology g shutting down at t

1. Introduction

The decarbonisation of the electricity sector relies on Renewable Energy Sources (RES), which displace a large share of conventional synchronous generation [1], [2]. The consequence of this process highlights the need for two main layers of flexibility.

First, an increased amount of so-called *power/energy flexibility* [3] will require traditional and new assets to provide larger amounts of fast frequency response services. This is caused by the level of Natural Inertia (NI) dropping to critically-low levels due to RES not contributing to NI in their standard configuration [4].

Second, *transfer-capacity flexibility* [3] is needed for RES to provide environmental and financial diversity of potential generation supplies. This requires upgrades of the transmission network infrastructure. Hence, the European Commission aims to strengthen the role of interconnection by setting a minimum national target of interconnection capacity with neighbouring countries of 10% of the generation capacity by 2020 (up to 15% by 2030) [5]. The boost in the capacity can be achieved with AC overhead lines or HVDC interconnectors.

This paper focuses on multi-area systems connected through HVDC links only. A realistic case are power systems like in Great Britain (GB) that can only resort to HVDC interconnectors with Ireland (IR) and Continental Europe (CE) due to the long distances involved and the presence of maritime borders. In this case, projects already under construction and others in the pipeline will bring the HVDC cross-border interconnection capacity in GB from the current level of 4 GW to 15-20 GW by 2030 [6].

This kind of system exhibits particular features. Unlike with AC overhead lines, if two power networks are only connected via HVDC links, they remain asynchronous, i.e., the frequency dynamics in one system are decoupled from those in the other. In other words, in case of a generation fault in one area, only the NI available in that area can limit the frequency deviations, with no support from the NI in neighbouring areas. This feature is notably a concern for small power networks, e.g., in IR and GB. On the other hand, large systems such as in CE may exhibit less significant operational challenges [7], [8]. Hence, the ability to *locally* provide fast frequency response service becomes crucial. The coordination of the power consumption of Thermostatically Controlled Loads (TCLs) may represent an effective remedy to the lack of NI and act as a source of power/energy flexibility[1] [9]. The effectiveness of aggregate TCLs would highly depend on their *local* penetration, i.e., the amount of responsive TCLs in each area of the interconnected system.

1.1 The research gaps

This section provides an overview of the two main research gaps with respect to the operation of multi-area HVDC-connected power systems. The interplay between these flexibility needs and their potential providers has been overlooked. This is based on the so far valid assumption that the inter-area power flows of HVDC links only depend on the spread between production costs[2] [10]. This paradigm applies to both regulated and merchant HVDC assets. In fact, increased interconnection capacity should in principle facilitate the integration of RES in one area, as part of this generation is transferred to another area. However, investigating the benefits of increased HVDC interconnection capacity without recognising the NI-dependent frequency dynamics in each area may drive to misleading results, especially under future energy scenarios. If the NI in the first area drops below critical levels, part of the available RES shall be curtailed and the power flowing through the interconnector would reduce. Eventually, HVDC links may not be able to effectively provide *transfer-capacity flexibility* if requirements on *power/energy flexibility* are not properly met.

The first research gap calls for modelling advancements in power system scheduling routines, e.g., Security Constrained Unit Commitment (SCUC) models, in order to accurately recognise the interplay between power-energy flexibility and transfer-capacity flexibility.

The second research gap is the ability to define the right price signals in order to positively affect the operation of flexibility suppliers. The flexibility needs of the systems are often translated into requirements for commercially-available ancillary services[3]. However, the prices for the ancillary services are the result of tenders between the system operators and the ancillary service providers [11], [12]. Unlike wholesale energy prices, prices for ancillary services do not accurately reflect the particular system conditions. Typically, they are defined well ahead of time and the prices, once defined, do not vary with time. Hence, these prices represent the *market value* of the corresponding ancillary services. However, since the system will need additional flexibility in future [13], the *economic value* of these services is expected to grow.

In accordance with [14], the market value is the price that an asset/service would fetch in the marketplace; in other words, the market value is the minimum amount a consumer will pay for a good or service. On the other hand, the economic value instead represents the maximum amount of money a buyer is willing and able to pay for a good or service. Thus, economic value is often greater than the market value.

In the next section, a detailed literature review analyses the findings and assumptions in previous works in the light of the identified research gaps. In particular, the related works recalled below integrate the TCL or HVDC flexible operation in typical unit commitment or competitive market clearing models.

1.2 Related work

In the context of the features of the first research gap, the benefits of flexibility from HVDC interconnectors were investigated in various research papers. In particular, reference [15] deals with a pan-European formulation of the energy market including both AC and HVDC lines and focusing on internalisation of HVDC losses in the clearing process. The findings in [16] highlight the effectiveness of the GB-French interconnection in balancing supply and demand. An economic and secure operation of the system is obtained in [17] following an iterative

[1] Despite technical differences, other assets such as stationary electricity storage [55], [31] or electric vehicles [56] could provide similar support. This paper focuses on TCLs; however, most results can be extended to other forms of storage.

[2] Previous research (e.g. [41], [42]) has shown the capability for HVDC to provide fast frequency response services. However, current operation show higher margin gained with wholesale energy price differentials compared to the revenues for sparing part of the HVDC capacity for frequency response [10] (around 2-5 £/MWh [12]).

[3] The presence of a one-to-one relation between system needs and commercially available ancillary services may vary with the country by country. For instance, in IR conventional synchronous generators provide contribute to the NI of the system and they are rewarded for this through a relevant ancillary service [54]. This is not the case in GB, where there is no market-driven arrangement for providing synchronous units providing NI.

solution of a SCUC problem including HVDC. Techno-economic challenges faced by a multi-area European power system are proved to be partially solved by HVDC interconnection in [18]. Similarly, influential technical reports (e.g. [10], [19], [20]) assess the value of current and future HVDC projects neglecting the impact of the lack of NI in singles area of the interconnected system.

On the other hand, Aunedi *et al.* [21] demonstrated the potential system operational cost savings and CO_2 emissions reduction driven by the provision of primary frequency regulation from TCLs. A framework for the integration of demand response in energy markets is presented in [22]. An analytical model for characterising the dynamics of operating reserves provided by TCLs is introduced in [23]. The model is used for the evaluation of the power-system short-term reliability. A two-stage stochastic unit commitment model with aggregated TCLs providing the reserve service is proposed in [24], and similarly in [25] and [26]. A novel mechanism for bidding and clearing strategy which incorporates the internal TCL dynamics is presented in [27].

However, all the above-mentioned works did not capture the interplay between power/energy flexibility and transmission-capacity flexibility, also because they focus on TCLs or HVDC individually. Moreover, in some works (e.g., [27] and [15]) the power system scheduling only considers the energy supply-demand balance and neglects the impact of system requirements for various ancillary services on system operation. Alternatively (e.g., [24] and [17]), the generation commitment decisions and the allocation of ancillary services do not fully recognise the impact of the NI on post-fault frequency dynamics. Some of these issues were partially solved in [28] and [29]. However, these works focused on the value of TCL flexibility in an isolated power system, thus neglecting potential synergies and/or conflicts with flexible HVDC operation.

The SCUC model in [30] provides a preliminary assessment of the storage-HVDC interactions considering the fulfilment of NI-dependent frequency requirements. However, the model did not consider the local frequency dynamics at both ends of the HVDC link. This prevented the analysis of the more interesting and complex cases where both areas connected by the HVDC links are largely constrained by the lack of NI. Furthermore, previous works (e.g., [22], [21], [29]) included only one or few ancillary services in the power system scheduling model adopted. In this case, the advantages for the system operation (e.g. reduction in operation cost) arising from the flexibility of TCLs or HVDC links is over- or under-estimated.

Concerning the second research gap, previous models were not able to provide price signals to inform about the economic value for flexible assets and ancillary services. SCUC models are typically formulated as MILP optimisation problems (e.g., [30], [28], [31]). Although these models capture very accurately most of the actual system requirements, they often quantify the benefits of flexibility only by means of an overall indicator, i.e., the annual total cost savings. A more granular analysis of the time-dependent *marginal value*[4] of single asset-related parameters (penetration of TCLs, HVDC capacity etc.) or system level parameters (e.g. ancillary services) is limited. This is due to the inability to maintain an economic interpretation of Lagrange multipliers associated to constraints of the optimisation problem (e.g., as shadow prices) [32], [33]. The unit commitment model in [33] explores the advantages of linearized modelling frameworks. However, it does not determine marginal values for ancillary services in order to compare them to those currently cleared in traditional tenders. Moreover, the NI-dependent frequency dynamics are not considered; in addition, the transfer-capacity flexibility is neglected in a single bus-bar equivalent model. An initial attempt to determine time-dependent marginal value for frequency response services is in [29]. However, the commitment model is developed for a single-node system and neglects most of the typical features of scheduling routines. A different approach was pursued in [34] in order to define the utility function of frequency response services. However, the study does not fully consider commitment decisions and system dispatch. In addition, the frequency model adopted neglects the load damping effect, avoiding non-linearities in the frequency evolution.

1.3 Contributions

This paper addresses the research gaps by proposing a novel methodology that accurately recognises the relevant interplays between TCLs providing *power/energy flexibility* and HVDC links providing *transfer-capacity flexibility*. Moreover, the paper considers both the fundamental system technical needs and the economic/financial value of commercially-available ancillary services. In particular, this work contributes to the existing research providing the following key contributions:

I. A novel Quadratic Programming (QP) formulation of a multi-area HVDC-connected SCUC. The proposed QP improves the formulations in [33] and [29] as it accurately captures all the relevant system requirements

[4] In this work, the marginal value for TCL/HVDC at a given time t is to be intended as the reduction in system operational cost that is obtained if one additional unit of TCLs/HVDC is added to the system. Similarly, the marginal value at a given time t for an ancillary service is the reduction in system operational cost that is obtained if one less unit of that service is allocated, assuming the unitary amount of service is provided externally without any cost.

including minimum up/down time, start-up/shut down time and ramping constraints on generation technologies. In addition, commitment decisions are optimally evaluated considering:

- typical supply-demand balance and feasibility constraints on individual assets;
- system-level requirements for eight ancillary services related to generation/load outages. In particular, (i) NI, (ii) primary response, (iii) secondary response, and (iv) contingency reserve are evaluated against the maximum infeed generation loss. In addition, (v) high-frequency response and (vi) downwards contingency reserve refer to maximum loss of load, while the requirement of NI takes into account both cases [11] [35]. Moreover, two operating reserves, i.e., (vii) upwards reserve and (viii) downwards reserve, deal with RES uncertainty and variability [36].

II. Besides the energy cost differentials between connected areas, the optimal power flows through the HVDC links are, for the first time to the best of the authors' knowledge, optimally evaluated considering the spread of the intrinsic costs for providing security *locally*. These, in turn, largely depend on the spatial variation in NI and on the availability of RES and flexibility sources between the areas. This feature was not enabled in other works (e.g., [30], [15]). Results clearly demonstrate that the expected operation of HVDC interconnectors could significantly vary if the local reduction of NI and its consequent impact on frequency dynamics are properly considered or simply neglected.

III. The proposed model investigates the optimal simultaneous interplay between aggregate populations of TCLs located in each of the areas of the system and the HVDC links connecting them. In the light of the variety of ancillary services modelled, the proposed set-up allows for a novel analysis on the value for different layers of system flexibility needs (e.g., short-term power support vs. long term energy shifting). Hence, the proposed model is capable of highlighting the main drivers of techno-economic competition between different sources of flexibility, i.e., thermal storage with TCLs and HVDC links. To the best of the authors' knowledge, this detailed analysis was not fully produced in previous works.

IV. Thanks to the accurate QP formulation, the proposed SCUC problem clearly shows, for the first time, the system-level marginal value for different ancillary services, highlighting peculiar dependency on time. These results could inform reviews of grid codes/regulatory frameworks associated to the procurement of ancillary services. In parallel, this work could appraise the development of price mechanisms which best match the system-value of ancillary services and the rewards for flexible services' providers, based on their intrinsic flexibility features.

V. The proposed SCUC expands the results in [28] by developing a set of system level NI-dependent constraints on frequency dynamics that also includes large infeed load losses (i.e., causing upwards frequency deviations). Hence, the demand side response model for TCLs developed in [28] is modified to integrate new dynamics of the TCL thermal energy and power. It is worth noting that the individual TCL ability to comply with system-level profiles is ensured by the control strategy in [37].

VI. The proposed model is applied to a realistic low-carbon scenario for IR, GB and CE. Comprehensive case studies analyse the potential benefits of enabling TCL flexibility in different areas of the interconnected system. The potential benefits of increasing the overall HVDC capacity, according to future plans [5], [38], is also considered. Both cases are assessed individually or simultaneously i.e. when both TCLs and HVDC penetrations are augmented.

The rest of the paper is organised as follows. Section 2 provides a high level description of the model set-up and assumptions. Section 3 deals with the presentation of the ancillary services and the quantification of associated system level requirements. Section 4 recalls the modelling of aggregate TCLs and numerical translation of TCL flexibility into a set of constraints for the SCUC. The mathematical formulation of the multi-area SCUC is provided in Section 5. The case studies and the analysis of the results are described in Section 6. Finally, Section 7 concludes the paper providing a summary of the findings and relevant conclusions.

2. General context and high-level description of the model

This work focuses on multi-area power systems that are facing to different extents challenges due to the reductions in NI to accommodate an ever increasing amount of converter-interfaced technologies. In particular, an interconnected system is considered, whose areas are linked by HVDC lines. This set up becomes necessary in case of long distances between the areas and/or the presence of maritime borders. Under this configuration, the frequency dynamics in each area are decoupled from those in others. The framework in Fig. 1 is a practical example; the GB system is currently connected to the system in Ireland (IR) and to Continental Europe (CE) via HVDC links.

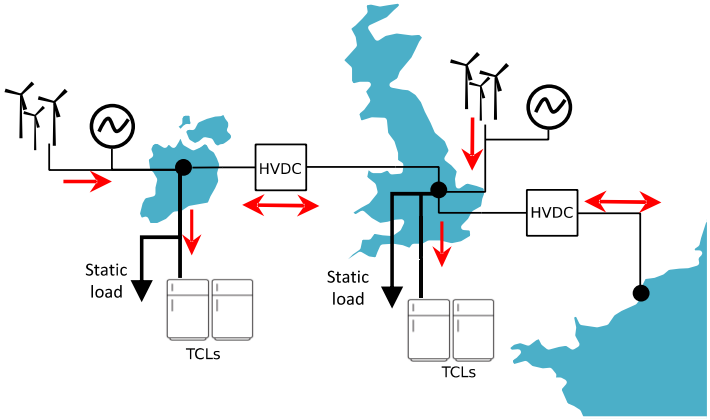

Fig. 1. Schematics of the multi-area HVDC-connected power system.

The typical operation of a HVDC interconnector relies on the basic *economic* principle that the energy flows from an area with lower electricity cost towards one with a higher electricity cost. An HVDC link is *efficiently* utilised when the power flow through it equals, almost at all times, the maximum rated capacity of the HVDC asset [10]. Moreover, HVDC links are usually built, owned and operated as regulated assets and they are exploited to boost the inter-area power flows, thus providing *transfer-capacity flexibility* [3]. Recently, interconnectors in GB act as merchant-assets, whose objective is to maximise their profit by exploiting the congestion surplus between two areas (e.g. GB and France). Note that the status of *regulated* assets or *merchant* assets does not change their fundamental operation, i.e., allocate their capacity to transfer energy between two areas [39]. In addition, the HVDC interconnection in GB has been allowed to participate in capacity auctions from 2015/16 for delivery in October 2017 [40]. The framework of capacity markets does not overlap with the system operation horizon. However, the allocation of part of the HVDC capacity for fast frequency response purposes is still not in place although initial research (e.g., [41], [42]) has assessed the necessary technology step-up to enable such capability[5].

Furthermore, the choice of investigating the interactions between the power networks in IR, GB and CE is particularly favourable, since the IR system is smaller than the GB one, which, in turn, is smaller compared to the size of the one in CE. This makes the technical needs for frequency control in each system quite different from the ones in the other systems.

Besides HVDC links, conventional generation and static load, the areas in Fig. 1 also include the presence of TCLs, whose operation can be coordinated to act as a *local* source of *power/energy flexibility* for the system [3]. Hence, the proposed SCUC minimises the system total operational cost by evaluating:

- generation commitment and dispatch decisions, also considering the retention of power headroom for a number of ancillary services;
- the TCL energy/power operation in coordination with the allocation of relevant ancillary services;
- the operation of the HVDC links connecting CE to GB and IR to GB.

Following a *centralised* approach, a single optimisation problem is proposed, where all the decision variables related to each of the areas in Fig. 1 are solved *simultaneously*. This formulation provides a lower bound for the aggregate operating costs of the power system in each area, since the operational choices of the systems are centrally planned. The mathematical description of the SCUC model and assumptions related to its formulation and implementation can be found in Section 5.

Moreover, it is worth pointing out that the commitment/dispatch problem is not explicitly modelled for CE. Hence, the operation of the CE-GB HVDC link also depends on cost-quantity curves for imported/exported energy. This assumption is based on the concept that commitment/dispatch decisions highly depend on the interplay between NI and frequency response services [30]. In this context, the CE system is considered as a whole, because of its high degree of AC-interconnection (and not only the French/Dutch systems which are actually connected to the GB [38]). However, the total rating of the CE-GB HVDC links is largely marginal compared to the size of the CE system[6], making any change to the HVDC operation negligible for the CE optimal dispatch and price. It follows that also the scheduling of ancillary services is neglected in CE.

[5] Nowadays, HVDC would still achieve higher margins chasing wholesale energy price differentials than the revenues for sparing part of the HVDC capacity for frequency response due to the quite low prices for these services (2-5 £/MWh [12]).

[6] Currently the CE-GB interconnection capacity is 3 GW [38] while the registered peak demand in CE is almost 550 GW [53].

Considering fast frequency response services and the reduction of NI, this issue is currently less concerning in CE than in it is GB and in IR [43].

Finally, the system in Fig. 1 only considers inter-areas power flows, thus neglecting the topology of the internal network of each area. For simplicity, transmission HVDC losses are also neglected.

3. Contingency and Operating ancillary services

Following a large and sudden generation/demand infeed loss, the system frequency would drop/rise below/above its nominal value $f_0 = 50$ Hz. The envelopes for admissible downwards/upwards post-fault frequency deviations are illustrated in Fig. 2a, while Fig. 2b zooms in on the initial part of the transient period. In GB [11] and IR [35], the maximum RoCoF equals ∓ 1 Hz/s and is evaluated over a window of t_ρ = 0.5 s. In other words, the frequency deviation after 0.5 s shall remain above/below $\Delta f_\rho = \mp 0.5$ Hz. Moreover, the thresholds for frequency deviations are Δf_{nad}=∓ 0.8 Hz (frequency nadir), before that a quasi-steady-state condition is reached at Δf_{qss} ∓ 0.5 Hz (i.e., frequency is no longer decreasing/increasing but has not recovered its nominal value yet). The full recovery to a pre-fault condition is completed through slower dynamics in 15-30 minutes (Fig. 2a).

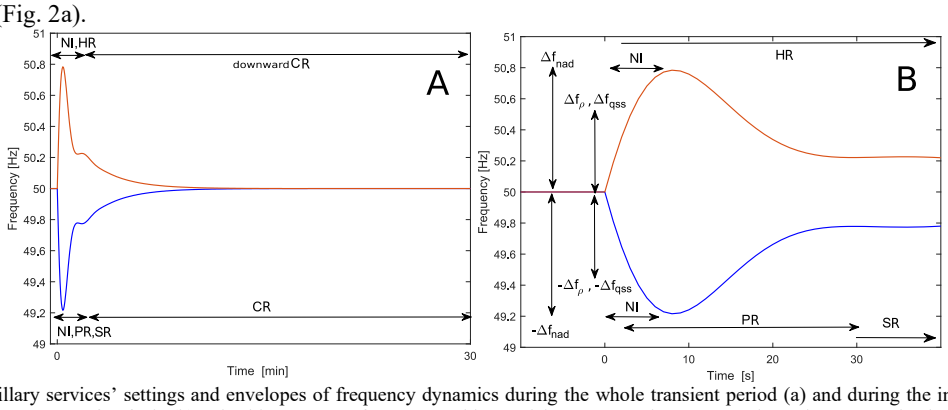

Fig. 2 Ancillary services' settings and envelopes of frequency dynamics during the whole transient period (a) and during the initial stages after the occurrence of a fault (b). The blue curve refers to a sudden and large generation outage, the red one to a load outage. The parameters used in the plots are consistent with [11] and [35].

The respect of the envelopes in Fig. 2 is guaranteed by deploying a number of ancillary services. This paper refers to *contingency ancillary services* to group those services provided, over different time scales, in response to a sudden and large generation/load outage. Although the particular settings of each of these services could differ from country to country, e.g., in terms of the delivery time and the duration of the service, their aims and structures are common [44].

The most rapid means to limit frequency drops is the *natural inertial response* (NI), although its support can be sustained only for very few seconds (see the corresponding window in Fig. 2a) [45]. Synchronous generators are the only providers of NI, deploying the kinetic energy stored in their rotating masses. The support from NI is overlapped and then taken over by the automatic injection/reduction of active power. Considering a generation loss, *primary response* (PR) is fully delivered by $t_{P_{GB}}$=10 s and $t_{P_{IR}}$=5 s and sustained for 20 s ([11], [35]). The mutual contribution of NI and PR allows frequency deviation to respect security standards on the RoCoF and on frequency nadir. Afterwards, *secondary response* (SR) supports the system. This service is fully provided within 30 s and is maintained for a longer time window (typically tens of minutes). The contribution of SR leads to the quasi-steady-state condition. Generation units would provide PR and/or SR by increasing their active power output, while demand-side units would procure the same effect by reducing their consumption (by $t_{H_{GB}}$=10 s [11]). On the other hand, in response to a positive frequency deviation, the objectives of PR and SR are achieved by a single automatic service named *high frequency response* (HR). Generators would need to reduce their output, while demand units increase theirs. Due to technical constraints, each technology acting on the power system may not provide the full range of services. Table 1 lists the relevant assumptions in this paper.

After a sudden generation fault, the recovery to a steady-state condition is enabled by the provision of the *contingency reserve* (CR). This service could be provided by *spinning* generators (i.e., already online) or by *standing* units, which were off-line before the fault and are brought to synchronism after the fault to provide CR. Given the generation mix considered in this work, only OGCT units can provide standing CR due to relatively short start-up time. On the other hand, following a sudden load reduction *downwards* CR is provided by generators that ramp-down their output. This service is provided necessarily only by units that were already on-line when the load reduction occurred. Note that TCLs do not provide CRs since these are energy-intensive

services, which do not well match typical TCL thermal dynamics. In fact, contingency reserves might be kept for long time intervals, e.g., hours. Moreover, the beginning of the time window for CRs overlaps with the end of the ones for HR and SR. This facilitates the taking over of responsive plants/TCLs (including their energy recovery [28]), allowing them to restore their response capability.

Table 1. Ability to provide contingency ancillary services.

Technology	NI	PR	SR	HR	CR	downwards CR
Nuclear	✓	–	–	–	–	–
Other fossil	✓	✓	✓	✓	✓	✓
Renewables	✗	–	–	–	–	–
TCLs	✗	✓	✓	✓	–	–
HVDC	✗	–	–	–	–	–

Ancillary services can (✓) or cannot (✗) be provided by each technology. Services denoted with '–' are not enabled in this paper for a certain technology but could be delivered provided certain technology set-ups. Concerning CR, only OCGT units provide standing reserve due to the small start-up time.

Concerning the services deployed after a generation loss, the system-level requirements for relevant contingency ancillary services recalls the methodology presented in [28] for NI, PR, SR and CR. In particular, a set of NI-dependent constraints effectively provide the requirements for NI and PR. Moreover, in this paper the same methodology is applied to derive system-level requirements for NI, HR and downwards CR, following a sudden and large load reduction. The structure of HR and downwards CR is therefore symmetric to the one of PR, SR and CR with respect to the pre-fault power condition (e.g. see Fig. 3). Moreover, the requirements for contingency ancillary services are evaluated, separately against the maximum generation/load *local* outages. Hence, each area is operated according to the *N-1 standard*. This is in line with HVDC not providing cross-border contingency ancillary services and the intrinsic characteristics of HVDC, which decouples the frequency dynamics of the connected areas.

This paper focuses primarily on the context of GB and evaluates its interactions with IR and CE. Hence, for simplicity, contingency ancillary services following a load outage in IR (i.e., HR and downwards CR) are not modelled. Finally, it is worth pointing out that the modelling of the very-fast responding service called *enhanced frequency response* [11], included in the GB context, is neglected, without affecting the fundamental findings of this work. In fact, the GB system requirement for such service is limited only to 200 MW and no increments have been adopted since 2016.

3.1 Operational reserves for wind uncertainty and variability

This paper focuses on wind generation as the main source of renewable energy. However, the following considerations can be extended to other renewable sources. In addition to the contingency ancillary services, the system-level requirements for the so-called *operational reserves* (ORs) are modelled to let the system operator cope with potential power mismatches between *expected* and *actual* wind levels [36]. Therefore, at a generic optimisation interval t, designated generators would deploy part or the whole allocated share of OR by means of a power increase if the actual wind happens to be lower than the expected level. On the other hand, downwards OR is provided, by means of a power reduction, if the actual wind is higher than the expected level. Moreover, the very same power headroom should not be allocated for both CR and OR.

Note that, the proposed SCUC problem does not perform *corrective actions*, e.g., intra-day adjustments of the system commitment/dispatch decisions as consequence wind power mismatches. The model implements *preventive actions* by allocating *enough* ORs to let the system cope with these issues, if needed.

At each time step, the system-level requirement for the ORs cannot account for all possible variations in wind output. For example, if the wind level at interval t and $t+1$ are expected to be 20 GW and 19 GW, respectively, it would be very unlikely that the actual wind realisation at $t+1$ happens to be nil or a very low level. Hence, the calculation of the system level requirements for OR relies on a Probabilistic Generation of Time-coupled Patterns methodology [46], which in this work depends on the Empirical Cumulative Distribution Function (ECDF) of the wind data, the expected wind level at each time step, and a pre-defined probability level. In practice, for each level of wind, the methodology provides the *upwards/downwards* wind variations (W_t and W_t^d respectively) from the expected wind level. In this paper, conventional generation technologies (excluding nuclear) are the designated providers of ORs. The procedure introduced above is performed with the iterative approach detailed in Algorithm 1.

Algorithm 1 Determination of system-level requirements for ORs (to be repeated $\forall k \in K$)

Step 1: Initialization

- Read $\boldsymbol{V} = \{V_1, \dots, V_y, \dots, V_Y\}$ the annual vector of wind ($Y = N \cdot T$ =17520 in p.u. so that $V_y = [0,1]$)
- Set N_q the number of quantiles and define the corresponding index $n_q = \{1, \dots, N_q\}$
- Compute $\vec{\boldsymbol{V}}$ sorting $\boldsymbol{V}$ in ascending order
- Set $\underline{\varepsilon}$ and $\overline{\varepsilon}$ as minimum/maximum probabilities levels (values in the paper $\underline{\varepsilon}$ =0.1 and $\overline{\varepsilon}$=0.9)

Step 2: Creation of ECDFs

- Determine quantiles' intervals $\boldsymbol{v}_{n_q}$ from $\vec{\boldsymbol{V}} \rightarrow \boldsymbol{v}_1 = [\min(V), q_1], \dots, \boldsymbol{v}_{n_q} = \left]q_{n_q-1}, q_{n_q}\right], \dots, \boldsymbol{v}_{N_q} = \left]q_{N_q-1}, \max(V)\right]$.
- Compute the ECDFs $F_1 \dots F_{N_q}$ from the data of corresponding quantile $\boldsymbol{v}_1, \dots, \boldsymbol{v}_{N_q}$
- Compute $\underline{\mathcal{R}}_{n_q} = F_{n_q}(\underline{\varepsilon})$ and $\overline{\mathcal{R}}_{n_q} = F_{n_q}(\overline{\varepsilon})$, $\forall n_q = 1 \dots N_q$

Step 3: Iterative solution

For $y = 1 \dots Y$

- Read V_y and identify the corresponding quantile $\boldsymbol{v}_{n_q \rightarrow V_y}$
- Compute $W_y = \left(V_y - \underline{\mathcal{R}}_{n_q}\right) \cdot \overline{G}_{wind,y}$
- Compute $W_y^d = \left(\overline{\mathcal{R}}_{n_q} - V_y\right) \cdot \overline{G}_{wind,y}$

end

Finally, in line with similar approaches in the literature [36], the proposed methodology calculates ORs as a function of the available wind. This may lead to an over-estimation of ORs' system requirements during those intervals characterised by a post-optimisation wind curtailment. However, the treatment of wind generation and associated reserves is not the main scope of the paper and the proposed methodology still allows for a conservative assumption. Moreover, the results of this work indicate a relatively high percentage of wind integrations, making the relevance of this issue negligible. Finally, in line with previous assumptions, the requirements and fulfilment of ORs are modelled only for the GB system.

4. Modelling and control of TCLs

An instructive description of TCL flexibility for system level applications was proposed in [37]. The aggregate TCL model is effectively reinterpreted as a battery-like storage unit. Hence, the thermal energy $E(\tau)$ evolves as:

$$\frac{dE(\tau)}{dt} = -\frac{1}{\eta}E(\tau) + \theta(\tau). \quad (1)$$

$$\underline{E} \leq E(\tau) \leq \overline{E} \quad (2) \qquad \underline{\theta} \leq \theta(\tau) \leq \overline{\theta} \quad (3)$$

This storage unit loses its stored energy with an intrinsic rate η^{-1} and it is replenished by the variable power consumption $\theta(\tau)$. Note that the storage unit cannot physically discharge electricity; it is only able to decrease or increase its consumption compared to its steady state consumption θ_0. Constraints on individual devices impose energy bounds (2). The cluster of individual TCLs described with (1)-(2), is controlled by means of an advanced strategy presented [37]. The particular controller implementation defines minimum/maximum power limits (3), which are constant with time. Any generic power profile $\theta(\tau)$ that is compatible with (2) and (3) is guaranteed to be feasible and non-disruptive for individual TCLs, avoiding the need for per-TCL simulations.

In this paper, two different populations of TCLs - one for GB, the other for IR - are smartly controlled to effectively engage in arbitrage with energy costs and support the fulfilment of system-level requirements for PR, SR and HR. Committing TCLs to perform energy arbitrage implies *actual* changes in their thermal energy profile, while, concerning frequency services, TCLs just have to maintain sufficient power/energy margins to ensure the *deliverability* of the services they have committed to.

At a generic interval t, in the example in Fig. 3, a power reduction θ_t (compared to the power level at θ_{t-1}) leads to an energy decrease (black solid curves). In case of a generation outage, the actual TCL consumption would drop following the blue dashed curves in order to provide $\tilde{P}_t$ and $\tilde{S}_t$. Consequently, the thermal energy would also reduce during the relevant time window Δt_a. The energy recovery phase follows, and it is performed, as in Fig. 3, by means of extra-power consumption, whose peak is above θ_t. This, in turn, depends on the amount of committed $\tilde{S}_t$ and the durations of Δt_b and Δt_c. Opposite dynamics occur if $\tilde{H}_t$ is actually provided, with power/energy following the red dashed curves.

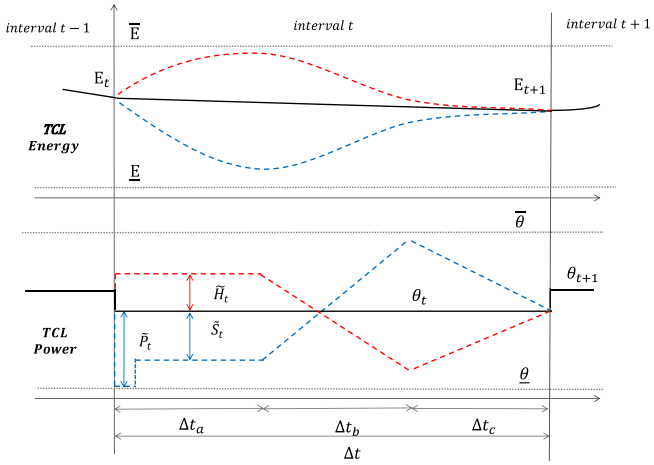

Fig. 3. Scheduling the TCL energy/power operation and allocation contingency ancillary services at a generic interval t. Under regular operation aggregate TCL follow the solid black curves. The provision of PR and SR requires TCLs to follow the blue dashed curves; the red dashed curves refer to the delivery of HR. Dotted lines are energy/power upper and lower bounds.

Two considerations arise. First, the allocation of SR and HR to TCLs requires increased system requirements for CR and downwards CR, respectively. Second, the TCL response model, as illustrated in Fig. 3, is constructed in such a way that, whether or not ancillary services are actually supplied by TCLs, the TCL energy and power consumption at the beginning of the next interval are kept at the pre-contingency level. This property guarantees the deliverability of frequency response services from TCLs, without depending on previous failure realizations.

5. The mathematical formulation of the SCUC model

The SCUC problem is presented, for the sake of simplicity, in a deterministic formulation, although a stochastic formulation is not impeded by the proposed methodology. Nonetheless, in order to improve the robustness of the results, the proposed UC is run for a number K of scenarios. In particular, single scenarios $k \in \{1 \dots K\}$ differ from each other by the actual wind availability (thus also associated ORs), demand and the CE-GB interconnection import/export costs.

Moreover, in line with other works (e.g. [33], [47]) the SCUC is presented by means of a QP formulation, which adopts only continuous decision variables. For example, considering a generic generation technology $g \in \mathcal{G}$ and assuming that the size of single plants relative to g is quite smaller than $\overline{G}_g$, typical ON/OFF commitment decisions can be extended to the fleet and expressed by continuous variables $\varphi_{g,t} \in [0,1]$. Authors in [33] demonstrated that this formulation still captures, with sufficiently high precision, all the relevant system scheduling requirements, e.g., the generation-demand balancing and allocation of ancillary services.

Moreover, a QP formulation of the SCUC is chosen since it ensures the continuity of the partial derivative of the objective function over a constraint's parameter. Hence, this quantity can be expressed by the Lagrange multiplier of the associated constraint. Due to this property, the Lagrange multipliers maintain the useful economic interpretation of shadow prices, i.e., marginal savings/costs for the system following unitary variations. For instance, this paper is able to clearly quantify the system marginal value of ancillary services (e.g., PR) to better understand the fundamental technical needs and interactions of the interconnected system in Fig. 1 [32]. Under MILP formulations, the interpretation of Lagrange multipliers as shadow prices cannot be necessarily guaranteed, due the non-continuous nature of some of the decision variables. In this case, non-trivial and time-consuming variational sensitivity analysis would be required [32].

In light of the assumptions previously mentioned, the objective of the proposed SCUC model is to minimise the total system operation cost expressed by the objective function $\hat{F}_k(\xi_k)$ in (5). Given the assumptions in Section 2, for all $g \in \mathcal{G}$, the function $\hat{F}_k(\xi_k)$ minimises the no-load costs, the production costs (a quadratic function of the dispatch level), which include the curtailment cost for wind generation, the start-up costs and the cost of managing the CE-GB HVDC interconnection. Note that there is no *explicit* formulation of any cost function for ancillary services. Considering, for example, generation technologies, these costs are *implicitly* accounted for as the financial loss for increasing the on-line capacity to maintain a certain power headroom for ancillary services.

Furthermore, in the problem formulation the thermal energies at the beginning (E_t) and the end (E_{t+1}) of each t are the actual decision variables. The TCL power consumption can be obtained via the linear function

$$\theta_t = \frac{E_{t+1} - \alpha_1 \cdot E_t}{\alpha_2} \tag{4}$$

which is the time-discrete solution of (1) at a generic interval t of duration Δt for a constant power $\theta_t(\tau) = \theta_t$. The numerical values of α_1 and α_2, so as of the parameters in TCL-related constraints (21)-(27) of the SCUC, are reported in Table 3 in Section 6. Let us assume that the TCL populations in IR and GB are made of the same types of units (domestic refrigerators, with built-in freezer compartment). The only difference is in the sizes of the populations $\widetilde{N}_x$ (and thus the energy/power levels). Moreover, considering Fig. 3, the duration of sub-intervals Δt_a, $\Delta t_b, \Delta t_c$ in GB equals the one in IR. Under these assumptions, the numerical values of the parameters in the constraints related to the TCLs in GB and IR are the same, since they are function of η and $\Delta t_a, \Delta t_b, \Delta t_c$, only.

Considering the cross-border interconnection, one-equivalent large HVDC link between IR and GB is modelled, rather than different interconnectors, individually. The same approach is adopted for the CE-GB links.

The SCUC problem (5)-(45) is solved for all the scenarios $k = \{1 \dots K\}$. Moreover, for each scenario k, N=365 individual simulations are carried out solving the proposed SCUC model over a 48 h time window with half-hourly time steps (i.e., Δt=30 min for 96 time steps in two days). Only the solution of the first 24 h is kept (discarding all the decisions beyond this limit). This is done to better account for minimum up/down time and starting up/shutting down time of conventional generation technologies. When moving from day n to $n+1$, commitment and dispatch decisions are adjusted, and inter-temporal constraints are properly maintained. Note that, for compactness of the notation, the dependency on k and n is no longer shown beyond the objective function (5). The dependency on n is reintroduced in (45) as necessary.

5.1 The mathematical formulation

The minimisation of the objective function is expressed as follows:

$$\min_{\xi_k} \hat{F}_k(\xi_k) = \sum_{n=1}^{N} \left\{ \sum_{t=1}^{2T} \sum_{g \in \mathcal{G}} \Delta t \cdot \left[c_g^{nl} \cdot \varphi_{g,t} + c_g^{lp} \cdot G_{g,t} + c_g^{ql} \cdot {G^2}_{g,t} \cdot \Delta t + c_g^{su} \cdot \chi_{g,t} + c_t^{\mathrm{I}} \cdot \mathrm{I}_t \right] \right\}_n \tag{5}$$

subject to $\forall t \in \{1 \dots 2T\}$ and $\forall g \in \mathcal{G}$ and $\forall x \in \{\mathrm{GB}, \mathrm{IR}\}$:

$$\varphi_{g,t} + \chi_{g,t} + \psi_{g,t} + \zeta_{g,t} \leq 1 \tag{6}$$

$$\varphi_{g,t} \geq 0 \tag{7a}$$

$$\chi_{g,t} \geq 0 \tag{7b}$$

$$\psi_{g,t} \geq 0 \tag{7c}$$

$$\zeta_{g,t} \geq 0 \tag{7d}$$

$$\varphi_{g,t+1} - \varphi_{g,t} = \chi_{g,t-t_g^{su}} - \psi_{g,t} \tag{8}$$

$$\varphi_{g,t} \leq 1 + \zeta_{g,t} - \sum\nolimits_{t-(t_g^{sd}+t_g^{d}-1)}^{t} \psi_{g,t} - \sum\nolimits_{t-(t_g^{su}-1)}^{t} \chi_{g,t} \tag{9}$$

$$\varphi_{g,t} \geq \sum\nolimits_{t-(t_g^{su}+t_g^{u}-1)}^{t-t_{su}} \chi_{g,t} \tag{10}$$

$$0 \leq P_{g,t} \leq \pi_g \cdot \varphi_{g,t} \cdot \overline{G}_g \tag{11a}$$

$$P_{g,t} \leq \sigma_g \cdot \left(\varphi_{g,t} \cdot \overline{G}_g - G_{g,t}\right) \tag{11b}$$

$$0 \leq S_{g,t} \leq \pi_g \cdot \varphi_{g,t} \cdot \overline{G}_g \tag{12a}$$

$$S_{g,t} \leq \sigma_g \cdot \left(\varphi_{g,t} \cdot \overline{G}_g - G_{g,t}\right) \tag{12b}$$

$$-\varphi_{g,t} \cdot \overline{G}_{g,t} \cdot \mu_g \cdot \Delta t \leq G_{g,t+1} - G_{g,t} \leq \varphi_{g,t+1} \cdot \overline{G}_{g,t+1} \cdot \mu_g \cdot \Delta t \tag{13}$$

$$\sum\nolimits_{g \in \mathcal{G}} G_{g,t} - \sum\nolimits_{x} \theta_{x,t} + \mathrm{I}_t = \sum\nolimits_{x} L_{x,t} \tag{14}$$

$$\left(\sum\nolimits_{g \in \mathcal{G}_x} P_{g,t} + \tilde{P}_{x,t}\right) t_\rho^2 - 2\Gamma_x \cdot t_\rho \cdot t_{P_x} + \frac{4\Delta f_\rho \cdot t_{P_x}}{f_0} \cdot \left[\sum\nolimits_{g \in \mathcal{G}_x} \left(h_g \cdot \overline{G}_{g,t} \cdot \varphi_{g,t}\right) - \Gamma_x \cdot h_{\Gamma_x}\right] \geq 0 \tag{15a}$$

$$\left(\sum_{g\in\mathcal{G}_x} P_{g,t} + \tilde{P}_{x,t}\right)\cdot\frac{\sum_{g\in\mathcal{G}_x}\left(h_g\cdot\overline{G}_{g,t}\cdot\varphi_{g,t}\right)-\Gamma_x\cdot h_{\Gamma_x}}{f_0}\geq Q_x\left(t_{P_x},\Gamma_x,L_{x,t},D_x\right) \tag{15b}$$

$$\sum_{g\in\mathcal{G}_x} S_{g,t}+\tilde{S}_{x,t}\geq\ \Gamma_x - D\cdot\ L_{x,t}\cdot\Delta f_{qss} \tag{16}$$

$$\sum_{g\in\mathcal{G}_x} C_{g,t}+\sum_{g\in\mathcal{G}_{x,\mathrm{OCGT}}}\zeta_{g,t}\cdot\mu_g\cdot\overline{G}_g\cdot\Delta t_b\geq\Gamma_x+\alpha_5\cdot\tilde{S}_{x,t} \tag{17}$$

$$0\leq C_{g,t}\leq\ \varphi_{g,t}\cdot\overline{G}_{g,t}\cdot\ \mu_g\cdot\Delta t_b \tag{18}$$

$$-\overline{I}_{\mathrm{CE}}^{\mathrm{GB}}\leq I_t\leq\overline{I}_{\mathrm{CE}}^{\mathrm{GB}} \tag{19}$$

$$\underline{E}_x\leq\ E_{x,t}\leq\overline{E}_x \tag{20}$$

$$\underline{\theta}_x\leq\theta_{x,t}\leq\overline{\theta}_x \tag{21}$$

$$0\leq\tilde{P}_{x,t}\leq\theta_{x,t}-\underline{\theta}_x \tag{22}$$

$$0\leq\tilde{S}_{x,t}\leq\theta_{x,t}-\underline{\theta}_x \tag{23}$$

$$\alpha_3\cdot E_{x,t}+\alpha_4\cdot\left(\theta_{x,t}-\tilde{S}_{x,t}\right)\geq\underline{E}_x \tag{24}$$

$$\theta_{x,t}+\alpha_5\cdot\tilde{S}_{x,t}\leq\overline{\theta}_x \tag{25}$$

$$\alpha_6\cdot E_{x,t}+\alpha_7\cdot\theta_{x,t}+\alpha_8\cdot\tilde{S}_{x,t}\leq\overline{E}_x \tag{26}$$

$x\in\{\mathrm{GB},\mathrm{IR}\}$:

$$\frac{1}{T}[\alpha_9\cdot E_{x,1}+\sum_{t=2}^{T}E_{x,t}\ +\alpha_{10}\cdot E_{x,(T+1)}]=E_{x,0} \tag{27a}$$

$$\frac{1}{T}[\alpha_9\cdot E_{x,(T+1)}+\sum_{t=T+2}^{T}E_{x,t}\ +\alpha_{10}\cdot E_{x,2T}]=E_{x,0} \tag{27b}$$

$t\in\{1\ldots2T\}$ and $g\in\mathcal{G}_{\mathrm{GB}}$ and $\forall x\in\{\mathrm{GB}\}$:

$$0\leq\widetilde{H}_{x,t}\leq\overline{\theta}_x-\theta_{x,t} \tag{28}$$

$$\alpha_3\cdot E_{x,t}+\alpha_4\cdot\left[\theta_{x,t}+\widetilde{H}_{x,t}\right]\leq\overline{E}_x \tag{29}$$

$$\theta_{x,t}-\alpha_5\cdot\widetilde{H}_{x,t}\geq\underline{\theta}_x \tag{30}$$

$$\alpha_6\cdot E_{x,t}+\alpha_7\cdot\theta_{x,t}-\alpha_8\cdot\widetilde{H}_{x,t}\geq\underline{E}_x \tag{31}$$

$$\left(\sum_{g\in\mathcal{G}_{\mathrm{GB}}} H_{g,t}+\widetilde{H}_{x,t}\right)t_\rho^2-2\Lambda_x\cdot t_\rho\cdot t_{H_x}+\frac{4\Delta f_\rho\cdot t_{H_x}}{f_0}\cdot\sum_{g\in\mathcal{G}_{\mathrm{GB}}}\left(h_g\cdot\overline{G}_{g,t}\cdot\varphi_{g,t}\right)\geq 0 \tag{32a}$$

$$\left(\sum_{g\in\mathcal{G}_{\mathrm{GB}}} H_{g,t}+\widetilde{H}_{x,t}\right)\cdot\frac{\sum_{g\in\mathcal{G}_x}\left(h_g\cdot\overline{G}_{g,t}\cdot\varphi_{g,t}\right)}{f_0}\geq Z_x\left(t_{H_x},\Lambda_x,L_{x,t},D\right) \tag{32b}$$

$$\sum_{g\in\mathcal{G}_x} H_{g,t}+\widetilde{H}_{x,t}\geq\ \Lambda_x - D\cdot\ L_{x,t}\cdot\Delta f_{qss} \tag{33}$$

$$\sum_{g\in\mathcal{G}_{\mathrm{GB}}} C_{g,t}\geq\Lambda_x+\alpha_5\cdot\widetilde{H}_{x,t} \tag{34}$$

$$G_{g,t}+max\left(P_{g,t},S_{g,t}\right)+C_{g,t}+O_{g,t}\leq\varphi_{g,t}\cdot\overline{G}_g \tag{35}$$

$$G_{g,t}-H_{g,t}-C_{g,t}^d-O_{g,t}^d\geq\gamma_g\cdot\varphi_{g,t}\cdot\overline{G}_g \tag{36}$$

$$0\leq H_{g,t}\leq\ \pi_g\cdot\varphi_{g,t}\cdot\overline{G}_g \tag{37a}$$

$$H_{g,t}\leq\ \sigma_g\cdot\left(G_{g,t}-\gamma_g\cdot\varphi_{g,t}\cdot\overline{G}_g\right) \tag{37b}$$

$$C_{g,t}^d\leq\ \varphi_{g,t}\cdot\overline{G}_{g,t}\cdot\ \mu_g\cdot\Delta t_b \tag{38}$$

$$0\leq O_{g,t}\leq\ \varphi_{g,t}\cdot\overline{G}_{g,t}\cdot\ \mu_g\cdot\Delta t \tag{39}$$

$$O_{g,t}^d\leq\ \varphi_{g,t}\cdot\overline{G}_{g,t}\cdot\ \mu_g\cdot\Delta t \tag{40}$$

$$\sum_{g\in\mathcal{G}_{\mathrm{GB}}} O_{g,t}\geq\ W_t \tag{41a}$$

$$\sum_{g\in\mathcal{G}_{\mathrm{GB}}} O_{g,t}^d\geq\ W_t^d \tag{41b}$$

$t\in\{1\ldots2T\}$ and $g\in\mathcal{G}_{\mathrm{IE}}$ and $\forall\in\{\mathrm{IR}\}$:

$$G_{g,t} + max\left(P_{g,t}, S_{g,t}\right) + C_{g,t} \leq \varphi_{g,t} \cdot \overline{G}_{g,t} \tag{42}$$

$$G_{g,t} \geq \gamma_g \cdot \varphi_{g,t} \cdot \overline{G}_{g,t} \tag{43}$$

$$L_{x,t} + \theta_{x,t} - \overline{I}_{\mathrm{GB}}^{\mathrm{IR}} \leq \sum\nolimits_{g \in \mathcal{G}_{\mathrm{IE}}} G_{g,t} \leq L_{x,t} + \theta_{x,t} + \overline{I}_{\mathrm{GB}}^{\mathrm{IR}} \tag{44}$$

$\forall n \in \{2 \dots N\}$ and $\forall x \in \{\mathrm{GB}, \mathrm{IR}\}$

$$Z_1^n = Z_T^{n-1} \tag{45a}$$

$$E_{x,1}^n = E_{x,T+1}^{n-1} \tag{45b}$$

Constraints (6)-(7) define upper and lower limits for the decision variables related to the different components of the capacity of each generation technology. Moreover, (8)-(10) introduce inter-temporal constraints as function of the $t_g^{sd}, t_g^d, t_g^{su}$ and t_g^u for each generation technology. The amount of PR allocated by each generation technology is limited by the headroom in (11a) and the slope linking the PR with the dispatch level (11b). The same structure applies to the allocation of SR (12). Constraint (13) accounts for typical generators' ramp-rates when increasing and decreasing their output. The system generation-load balance is guaranteed by (14), which will be complemented by additional constraints on the power flows through the interconnectors (19) and (44). Constraints (15) ensure the allocation of sufficient mix of NI and PR from generators and TCLs in order to limit the post-fault RoCoF and the frequency nadir after a sudden and large generation outage. Note that the formulation of these constraints was presented in [30], [28], including relevant linearization techniques concerning (15b). The PR allocated by generators/TCLs is assumed to be linearly delivered by t_{P_x}. Moreover, (16) allocates SR to reach a quasi-steady state condition, accounting for the damping characteristic of the system load. Furthermore, spinning and standing CR is allocated in (17) to fully replace the Γ_x and to cope with the TCL energy payback as in [28]. Generators' ramp-rates happen to limit the maximum CR that each technology can provide in the relevant time window Δt_b (18). Upper and lower limits for the power flowing through the GB-CE HVDC link are ensured by (19). As arguable also from the objective function (5) a positive/negative value assumed by I_t implies a power flow from CE/GB and vice versa.

The TCL power/energy operation and the consequent allocation of PR and SR are reported in (21)-(26). These constraints reflect the general scheme of TCL flexibility illustrated in Fig. 3 and based on [28]. Moreover, equation (27) envisages that the average thermal energy across a 24 h interval has to be equal to the steady-state level E_0. Since the optimization interval is 48 h), this constraint is applied twice.

The following constraints refer to the GB area only. In accordance with Fig. 3, equations (28)-(31) define the boundaries for the allocation of HR to TCLs. These constraints follow, symmetrically, the same methodology concerning PR and SR. Similarly, equation (32) reflect (15) while ensuring the respect of post-fault frequency dynamics following Λ_x. Differently from in (15a), the load reduction in (32a) does not lead to a further post-fault reduction of NI. Moreover, equations (33) and (34) extend the objectives of (16) and (17). In particular, equation (33) complements the system-level requirement for HR to ensure a quasi-steady state condition, while (34) deals with the procurement of enough downwards CR, also including the TCL energy recovery pattern after the provision of HR.

The sum of the dispatch level and the total upwards spinning headroom for different ancillary services is maintained below the online capacity by means of (35). On the other hand, provided that a certain amount of generation capacity (for a given technology) is actually online, the dispatch level in (36) has to be greater than a certain percentage of the online capacity, also considering the possible power reduction after the provision of HR and downwards CR/OR. Considering HR, the structure of (37) is similar to the one in (11) and (12), while (38) constrains the capability for downwards CR. The capabilities for ORs are defined in (39) and (40). The fulfilment of system level requirements for the OR is guaranteed by (41), where W_t and W_t^d are determined through the application of Algorithm 1 in Section 3.

As mentioned in Section 3, upwards frequency deviations following load reductions and ORs are not modelled in IR. Hence, equations (42) and (43) rearrange (35) and (36) respectively to these assumptions. Furthermore, the constraint (44) complements the application of (14) and (19) making sure that the generation level in IR, including the power flow through the GB-IR HVDC link, can satisfy the aggregate inflexible load and the TCL consumption in IR.

Finally, when moving from day n to $n+1$, the constraints (45) implement the continuity of the solutions. Note that Z_t^n in (45a) is defined as the subset of ξ_k referring to the generic time step t of the generic day n. The subset does not include $E_{x,t}^n$ $\forall x = \{\mathrm{GB}, \mathrm{IR}\}$.

6. Case studies and results

The generation mix reflects a number of typical low-carbon scenarios of the GB and IR and are inspired by [6] and [48]. The half-hourly measures of inflexible system load, wind availability (for both GB and IR) and CE-GB import/export costs for each scenario $k = \{1 \dots K\}$ with K=20 are from EDF Energy. The authors used them only for research purposes and as input quantities with respect to the SCUC model. Although being different on a daily/half-hourly base, each scenario preserves typical seasonal variability and correlations exhibited historically. Hence, for all the N days and K scenarios, Fig. 4a and Fig. 4b show the box and whisker plots of the inflexible load in GB and IR. Wind availabilities are shown in Fig. 4c (in per unit of the installed capacities 37 GW in GB and 4 GW in IR). The median quantities are almost the same, while the IR data show a slightly higher variability. The figure also shows the distribution of the system-level requirements for ORs in GB, obtained with Algorithm 1 in Section 3. Finally, Fig. 4c also illustrates the distribution of the c_t^{I} (in p.u. of the maximum quantity) with a median quantity which corresponds almost to 60£/MWh. The characteristics of the thermal generation technologies are reported in Table 2.

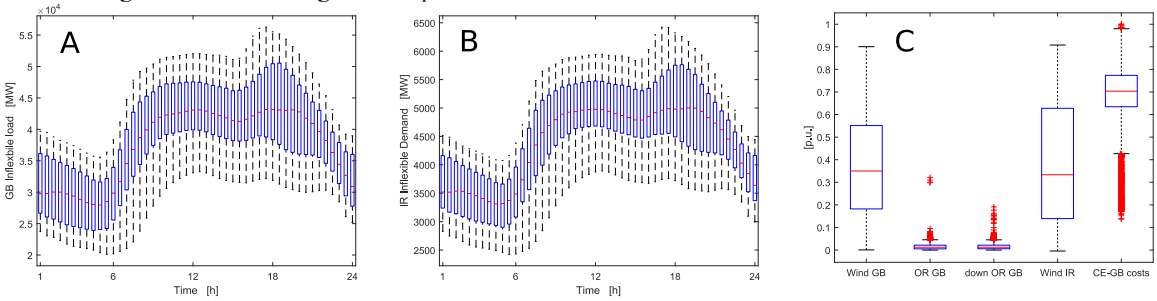

Fig. 4. Distributions of Inflexible load in GB (a), IR (b), CE-GB interconnection costs and wind availabilities in GB and IR (c).

Table 2. Characteristics of thermal generation technologies.

Technology		$\overline{G}_g$ [GW]	N_g^u	c_g^{nl} [k£/h]	c_g^{lp} [£/MWh]	c_g^{ql} [£/(MWh)^2]	c_g^{su} [k£/h]	t_g^{sd} [h]	t_g^{d} [h]	t_g^{su} [h]	t_g^{u} [h]	π_g	σ_g	μ_g [h^{-1}]	h_g [s]	ν_g
GB	Nuclear	9.6	6	0.25· N_g^u	5	0.005	0	24	24	24	24	-	-	-	5	-
	OCGT	28	90	9· N_g^u	110	0.015	1· N_g^u	0.5	0.5	0.5	0.5	0.1	0.6	0.175	4	0. 35
	CCGT	32	40	8· N_g^u	45	0.005	32· N_g^u	4	4	4	4	0.1	0.4	0.05	4	0.5
IR	OCGT	3	10	9· N_g^u	110	0.02	1· N_g^u	0.5	0.5	0.5	0.5	0.1	0.6	0.175	4	0. 35
	CCGT	5	6	8· N_g^u	45	0.01	32· N_g^u	4	4	4	4	0.1	0.4	0.05	4	0.5

Let us consider a wind curtailment cost[7] of 75 £/MWh [49]. Additional system level parameters are Δt_a=Δt_b=Δt_c=10 min [28]. The capacities of the HVDC links are $\overline{I}_{\mathrm{GB}}^{\mathrm{IR}}$ =1 GW and $\overline{I}_{\mathrm{CE}}^{\mathrm{GB}}$=5 GW. The amount relative to CE-GB considers the ratings of HVDC links already in operation (3 GW) and the additional contribution of the ElecLink and NEMO projects to be delivered in 2020 [38]. Moreover, Γ_{GB}=1.8 GW, Γ_{IR}=0.5 GW, Λ_{GB}=1.4 GW, $h_{\Gamma_{\mathrm{GB}}}$=5 s, $h_{\Gamma_{\mathrm{IR}}}$= 4 s, and D=0.5 Hz^{-1} [30], [50]. The numerical values of the parameters related to TCLs are shown in Table 3. Note that the quantities in the first row apply to both IR and GB. Concerning the second row, the first numbers refer to GB, the second ones to IR.

The SCUC problem is solved with the *quadprog* function of Matlab R2019b. Simulations are carried out on an Intel i7-8750H 2.2 GHz processor with 16 GB RAM. On average, the simulation time is 0.5 h for each scenario k.

Table 3. Parameters related to TCLs.

α_1	α_2 [h]	α_3	α_4 [h]	α_5	α_6	α_7	α_8	α_9	α_{10}
0.9048	0.4758	0.9672	0.1639	1.4402	0.9355	0.3225	-0.1214	0.4917	0.5083
$\overline{\theta}_x$ [GW]	$\underline{\theta}_x$ [GW]	$\overline{E}_x$ [GWh]	$\underline{E}_x$ [GWh]	$\theta_{x,0}$ [GW]	$E_{x,0}$ [GWh]	η_x [h]			
8.9/1.8	1.9/0.4	18.2/3.6	15.4/3	3.5/0.7	16.8/3.3	5/5			

The descriptions of the case studies considered in this paper are listed in Table 4. All the results in the next sections refer to average quantities across all the K scenarios.

[7] Concerning wind generation costs in IR and GB, c_g^{nl}=c_g^{ql}=0 and c_g^{lp}=-75 £/MWh. After solving problem (5)-(45), the term $£\ 75 \cdot \Delta t \cdot \sum_{n=1}^{N} \sum_{t=1}^{T} \left(\overline{G}_{wind,t,n}\right)$ is added to the total annual operation cost, so that the operational cost accounts only for wind generation actually curtailed.

Table 4. Description of the case studies

Case Study	Description
BC	All the assumptions above apply. TCLs in GB and IR are assumed inflexible (i.e., at each interval t, $\theta_{x,t} = \theta_{x,0}$) and do not provide any ancillary service.
CS1	same as in BC but TCLs in GB are flexible (i.e., operated as in Fig. 3).
CS2	same as in BC but TCLs in IR are flexible.
CS3	same as in BC but TCLs in GB and IR are flexible.
CS4	same as in BC with $\overline{I}_{GB}^{IR}$ increased by 1.634 GW. This value equals the response capability of TCLs in GB from a steady-state level i.e. $\theta_{GB,0} - \underline{\theta}_{GB}$=1.634 GW.
CS5	same as in BC with $\overline{I}_{CE}^{GB}$ increased by 1.634 GW.
CS6	same as in BC with $\overline{I}_{CE}^{GB}$ and $\overline{I}_{GB}^{IR}$ increased by 1.634 GW.
CS7	it combines the assumptions of CS3 and CS6.

6.1 High level results

The annual total operational cost savings (relative to the BC) are presented in Fig. 5a. In the BC, the annual total operational cost is b£ 24.5. Results show that enabling TCL flexibility (CS1-CS3) is more beneficial than increasing the HVDC capacity (CS4-CS6). Hence, from an overall system perspective, the benefits for enabling power/energy flexibility exceeds the one for transfer-capacity flexibility. In CS4, the large increase in the GB-IR HVDC capacity (1634 MW in addition to the 500 MW in BC) allows for just a 0.1% reduction in total system costs. It is worth noting that the cost savings in CS7 are only slightly lower than the sum of those in CS3 and CS6, implying fundamental synergies between the two layers of flexibility provided by TCLs and HVDC links.

Furthermore, Fig. 5b shows the partitioning of total operational costs. Considering CS1 (or CS2), it is possible to infer that the provision of TCL flexibility in GB (or IR) reduces the weight of generation cost in GB (or IR) with respect to the total cost, while it increases the weight of generation cost in IR (or GB). Moreover, it is worth noting that there are no significant changes to the costs' repartition when HVDC capacities are increased individually or simultaneously. Finally, those case studies that enable the largest cost savings (i.e., CS1, CS3 and CS7), reveal a significant increase in the weight of the CE-GB HVDC costs component.

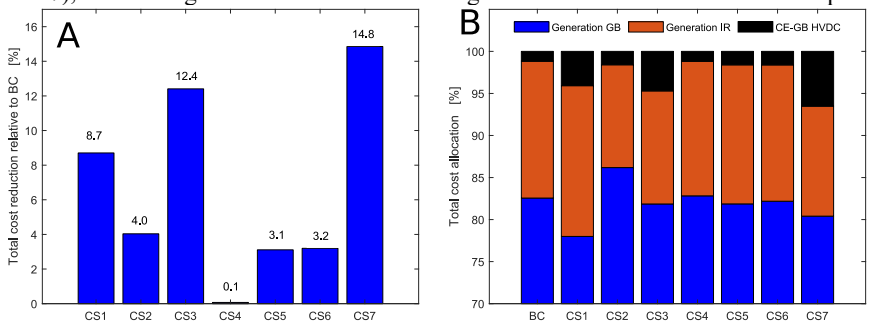

Fig. 5 (a) annual total operational cost reductions relative to BC; (b) allocation of annual total operational cost among the three components.

Focusing on HVDC, an important metric to consider is its marginal value, as it provides the upper cost limit for HVDC deployment for a given amount of installed capacity. Only if the marginal cost necessary to install one additional unit of HVDC is lower than the corresponding marginal value, should further HVDC be installed. From the results in Fig. 5a concerning CS4 it is possible to infer that marginal value for the GB-IR link is around 15000 £/MW. Similarly, considering CS5, the marginal value of the CE-GB link is around 47000 £/MW[8]. On the other hand, considering the assumptions on the capital and operational costs for HVDC links in [20] and [51], the marginal costs[9] for a unitary increase (1 MW) of HVDC capacity are much higher than the marginal values and they are around 415000 £/MW and 520000 £/MW for the GB-IR and CE-GB links, respectively.

In addition, higher degrees of flexibility imply higher reductions in wind curtailments (Table 5). Once again, the bottleneck limiting the wind integration is not a poor transfer-capacity infrastructure but the local reduction in NI. In fact, CS1, CS3 and CS7 reach the most relevant variations compared to BC. Note that CS2 and CS4

[8] Considering the cost reductions in Fig. 5a, the total operational cost being 24.5 b£ (in the BC) and the increment in capacity for CS4 and CS5 equal to 1634 MW, the marginal values are calculated as (0.031×24.5)/1634=46450£/MW (CE-GB link) and (0.011×24.5)/1634=14933£/MW (GB-IR link).

[9] The capital and operation costs are assumed to be in total 3000 €/MW/km, the length of the GB-IR link is assumed to be 160 km as the GreenLink project. Similarly, 200 km is the length of the new IFA 2 link between CE and GB [51]. The exchange rate is assumed to be 1£=1.15€.

allows for large reductions in wind curtailment but only relative to IR area. In fact, these two case studies increase the level of flexibility for IR by smartly controlling local TCLs (CS2) or allowing more wind energy to be transferred to GB via the increased capacity of the GB-IR HVDC link (CS4).

Table 5. Split of cost variations and wind curtailment variations relative to BC.

variations relative to BC	Case Study						
	CS1	CS2	CS3	CS4	CS5	CS6	CS7
System wind curtailment	-44.1%	-8.7%	-50.3%	-0.43%	-18.9%	-19.4%	-61.5%
GB wind curtailment	-46.1%	-6.1%	-49.5%	3.7%	-19.8%	-16.0%	-59.8%
IR wind curtailment	-0.13%	-65.4%	-69.2%	-92.5%	-0.1%	-97.1%	-99.1%

6.2 Focus on HVDC operation

The following results focus on the operation of the HVDC links. To this end, Fig. 6a-b show the annual energy exchanges through (a) the CE-GB HVDC link, and (b) the GB-IR HVDC link. On the other hand, Fig. 6d shows the *utilisation indices* relative to the two interconnectors defined as the sum over one year of the energy flowing across the HVDC link (in whatever direction, i.e., positive quantities) over the maximum energy that could annually flow, i.e., if the links were transferring energy at their maximum capacity at all times.

In Fig. 6a, the case studies concerning to TCL flexibility (CS1-CS3) show a reduction in the energy transferred from GB to CE, while it increases in the opposite direction. Moreover, note that the annual utilisation indices, relative to these case studies and to the CE-GB HDVC link in Fig. 6d, remain almost the same as in the BC (around 80%). Although the total energy flow does not grow, the operation of the HVDC link is *overall* more efficient, as demonstrated by the cost reductions in Fig. 5a. Case studies with augmented CE-GB HVDC capacity (CS5-CS6) show higher annual flows than in the BC. However, this increase does not prevent the corresponding utilisation indices in Fig. 6d from reducing, as consequence of the higher interconnection capacity (i.e., the numerator of the utilisation index increases by a certain quantity, but the denominator has grown by an even larger one). Finally, CS7 replays these two trends, since it consists of a combination of the settings of CS3 and CS6.

In parallel, under the most cost-effective scenarios, the energy exchange from IR to GB increases, with a reduction in the flows in the opposite direction. The results relative to CS1 and CS2 in Fig. 6b offer an interesting consideration. Considering IR, when the TCL flexibility is available *locally* (CS2), it is possible to dispatch more wind energy in IR compared to the BC (also demonstrated by the high reductions in wind curtailments in the corresponding cell in Table 5) and transfer part of it towards GB. This of course requires reductions in the total energy from GB to IR. On the other hand, when TCL flexibility is available only *indirectly*, as only TCLs in GB are smartly controlled (CS1), the energy flow from IR to GB reduces compared to the BC, while the one from GB to IR increases. Hence, it is possible to conclude that granting flexibility only in one area has the effect of increasing the energy exports from that area to the one with less flexibility. Moreover, it is worth noting that increasing the HVDC capacities, either individually (CS4-CS5) or simultaneously (CS6), has the effect of increasing the energy exchange from GB to IR, causing its reduction in the opposite direction.

Overall, considering the corresponding quantities of utilisation indices in Fig. 6d, granting TCL flexibility in IR (CS2) and in both areas (CS3) allows for improvements of few percent points, compared to the BC. When the HVDC capacity increases (CS4, CS6 and CS7) the values drop below 30%. Moreover, the quantities of the utilisation index for the GB-IR link are significantly lower than those relative to the CE-GB one.

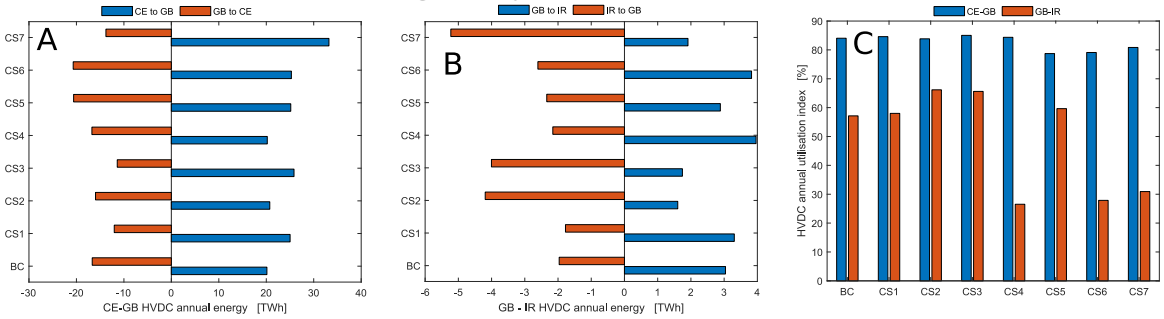

Fig. 6 Annual energy flows through (a) the CE-GB HVDC link, (b) the GB-IR HVDC link; (3) annual utilisation indices of HVDC links.

These results suggest interesting implications. The GB-IR HVDC capacity would be largely underutilised, since both the GB and IR areas are highly constrained by frequency dynamics (much more than CE). In other words, in low carbon isolated power systems (as in IR and GB), maintaining enough NI combined with PR (and

HR) becomes pivotal. To do so, especially during intervals characterised by low net demand, it would be convenient for both IR and GB systems to transfer energy across the HVDC link in order to increase *locally* the synchronous generation (thus the NI). However, the energy produced by synchronous technologies in one area, and transferred through a HVDC link, is seen as asynchronous generation in the receiving area (i.e., not contributing to the NI). This problem clearly cannot be solved by increasing the interconnection capacity and operating it under traditional mechanisms. Actually, the problem would be exacerbated as demonstrated by the utilisation index being below 30% in CS4.

Moving to the CE-GB HVDC link, it is worth noting that CE is not affected by issues on post-fault frequency dynamics (at least under the assumptions of this paper). From a centralised system-perspective, it would always be possible to accept generation from GB, brought online to facilitate the respect of local frequency issues, keeping the HVDC *sufficiently* utilised (around 80%). However, this should not be interpreted as an efficient solution and be used to justify (form an operational point of view) increased HVDC capacity over implementing local flexibility sources.

The median quantities (evaluated at each half-hourly time step) of the utilisation indices are shown in Fig. 7 for the GB-IR HVDC (a) and CE-GB HVDC (b) links. Considering Fig. 7a, it is worth noting that the CE-GB interconnector is often fully loaded in the BC and even when its capacity is augmented, i.e., CS6. However, the high negative flows during night hours may not necessarily imply an efficient operation of the system. Despite typically low import costs from CE, the generation in GB is brought on-line only to deal with local frequency dynamics. In fact, more cost-efficient case studies (e.g., CS3 and CS7) allows for reductions in *inefficient* flows (with utilisation indices during night hours reducing from 100% up to 20-40%).

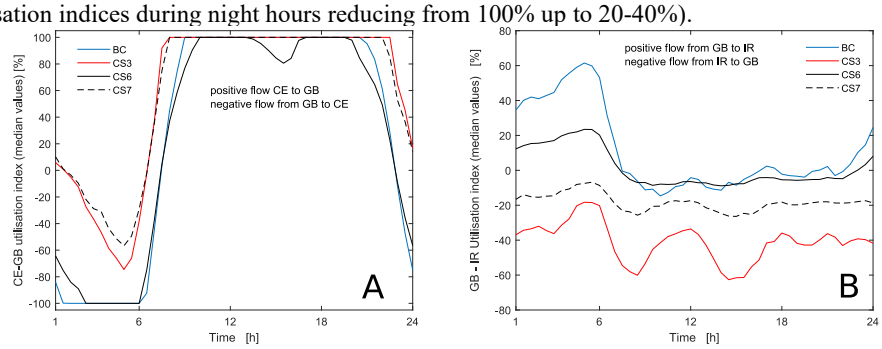

Fig. 7. Typical operation (relative to the maximum capacity) of the (a) CE-GB HVDC link and (b) the GB-IR HVDC link.

On the other hand, as of Fig. 7b the utilisation of the interconnector is overall limited, especially in certain hours (e.g. 09:00-22:00) under the BC and CS6). It is worth noting that the median quantities never reach upper/lower thresholds. The opposite trends between the power flows in BC and CS3, already shown in Fig. 6b, are also confirmed here in Fig. 7b, since the medians switches from positive quantities (i.e., typical flow from GB to IR) in BC to negative quantities (i.e., typical flow from IR to GB) in CS1.

In Table 6, the annual operation of HVDC links and corresponding utilisation indices obtained in the BC are compared to those of a case study with the same assumption of the BC except $\Gamma_{GB}= \Gamma_{IR}= \Lambda_{GB}=0$, i.e., where no contingency ancillary service is allocated. The assumptions of this case study reflect the typical understanding that the inter-area power flows of HVDC links only depend on the spread between production costs. When commitment and dispatch decisions no longer depend also on the available NI, but only on the spread of production costs, the directions of the HVDC power flow change directions. The power transferred from GB to CE reduces by a factor four, while it increases in the opposite direction. On the other hand, IR is now able to transfer its production to GB. The utilisation index of the CE-GB interconnector registers a small increase, while the one relative to the GB-IR HVDC link significantly grows. These results serve as a counterexample to show that any future strategy on expanding HVDC capacity that assesses HVDC operation and associated revenues only considering energy price differentials and neglects the technical *local* needs of the system (specifically the reduction of NI) is largely myopic.

It is worth pointing out that the annual utilisation indices for the no-contingency case are in line with those reported in a study commissioned by the GB regulatory authority (Ofgem) on the potential benefit for the GB system arising from an increase of the of interconnection capacity [52].

Table 6. Annual HVDC operation and utilisation indices.

Case study	annual energy flows [TWh]				annual utilisation index	
	CE to GB	GB to CE	GB to IR	IR to GB	CE-GB	GB-IR
BC	20.14	16.68	3.04	1.96	84.05%	57.15%
BC – no contingency	34.51	4.11	0.13	7.05	88.19%	82.08%

6.3 *Focus on TCL operation*

The TCL operation (half-hourly median quantities) is shown in Fig. 8. The leftmost figure refers to IR, the central to GB, and the rightmost to both. Moreover, in Fig. 8a-b, black solid line represents the optimal power profile of aggregate TCLs ($\theta_{x,t}$); the black dashed line is $\underline{\theta}_x$ (the upper bound is quite higher and is not plotted to preserve the readability of the figures). The red area is the allocated SR ($\tilde{S}_{x,t}$), while the sum of the red and grey areas corresponds to the allocated $\tilde{P}_{x,t}$. For the GB case only, the light blue area is the allocated $\tilde{H}_{x,t}$. The thermal energy profiles (in p.u. of the corresponding $E_{x,0}$) are shown in Fig. 8c. First of all, it can be noted that the maximum dispatchable PR is allocated at all the time steps ($\tilde{P}_{x,t} = \theta_{x,t} - \underline{\theta}_x$). This is an expected result, given the absence of energy-related constraints on PR allocation. Clearly, the same result does not apply to SR (and to HR also due to further considerations explained below), whose allocation varies during the day and is lower than the maximum dispatchable amount.

It is worth pointing out the typical daily pattern of the power profile and associated thermal energy. Aggregate TCLs tend to increase their consumption (above $\theta_{GB,0}$=3.5 GW and $\theta_{GB,0}$=0.7 GW) during the first part of the day and reduce it later. This behaviour may facilitate the allocation of PR, SR and HR where possible and, in parallel, the realisation of energy arbitrage. Results show that an increased TCL consumption enables larger allocation of PR and/or SR. This is registered during the first 10 hours of the day, when the system requirements for PR and SR and their corresponding marginal values (see Fig. 9) would be typically high due to low NI conditions. This is further justified by the generally low energy costs under these conditions. On the other hand, results show that, during hours with high demand conditions, TCLs tend to decrease their aggregate consumption, thus lowering the available response capability. This action is driven by the reduced system response requirements (several synchronous units online and thus large NI) and the higher energy costs.

Hence, it is possible to infer that the allocation of PR and/or SR and the realisation of energy arbitrage are characterised by a practical synergy.

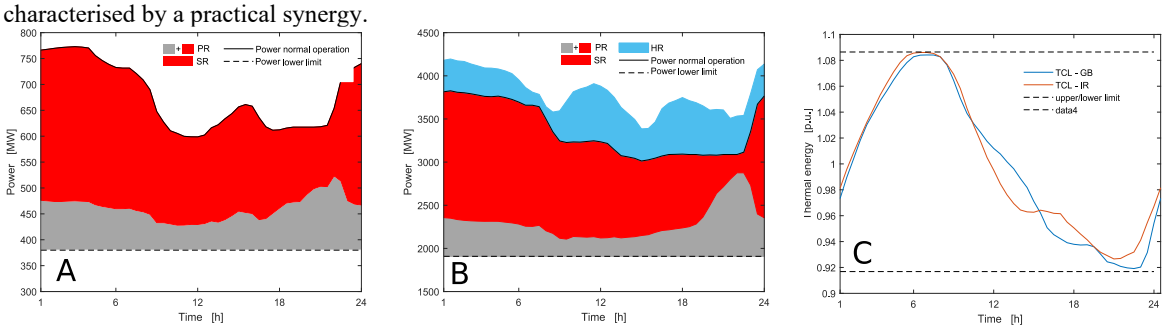

Fig. 8. TCL power profiles and services' allocation in (a) IR and (b) GB; (c) TCL thermal energy profiles (relative to $E_{x,0}$) in GB and IR.

As illustrated in Fig. 8b, similar synergic trends do not appear for the case of HR. During low inertia and low energy cost conditions, a significant allocation of HR would be made possible by a reduction of the TCL power consumption. However, TCLs would need to increase it later during subsequent high-energy cost conditions, despite overall lower system level requirements.

6.4 *Allocation of ancillary services*

The annual system-level allocation of the ancillary services is summarised in Table 7. The quantity for each case study represents the average quantity among all optimisation intervals. The table refers to the GB area only, although the analysis of the data below can be extended to the case of IR (for the ancillary services present on both areas). Thanks to the TCL flexibility CS1-CS3 and CS7 reach a large reduction in the committed NI compared to the BC. The other source of flexibility, introduced by augmenting the HVDC capacity, cannot provide similar benefits (so as CS2 when analysing GB results). In order to balance the reduction of NI, the GB allocation of PR grows; however, TCLs provide almost 50% of the total requirement, letting conventional generation in CS1, CS3 and CS7 reducing their PR allocation, compared to the corresponding quantities in other cast studies. The TCL flexibility is utilised to SR purposes, again reducing the share allocated to generators. Similar trends occur for the case of HR, although TCL participation is less remarkable (around 20% of the GB requirement as anticipated in Section 6.3).

Moving to the CR, two considerations arise. The case studies envisaging allocation of SR to TCLs require higher amount of CR (see (17)). As confirmed by previous results, the cost for this extra requirement is compensated by the large cost reductions enabled by TCL providing SR. Furthermore, in CS1, CS3 and CS7, the CR system requirement is largely met by standing generation (almost 80% of the total CR requirement), reducing the cost for extra CR. In fact, on the BC and other case studies, the need for NI made necessary that

spinning generation covered almost 85% of the total CR requirement. Similarly, the GB requirements for downwards CR increase in those case studies where shares of the HR requirements are allocated to TCLs.

Finally, in the BC the amounts of OR and downwards OR reach, on average, 545 MW and 551 MW, respectively. Note that these do not change with the case studies. The additional levels of flexibility introduced in CS1-CS7 simply let more cost-effective generation technologies fulfilling these requirements.

Table 7. Allocation of contingency ancillary services in GB.

Case	NI [MWs^2]	PR [MW]			SR [MW]		HR [MW]			CR [MW]			CR down [MW]
		Gen	TCL	tot	Gen	TCL	Gen	TCL	tot	Spin	Stand	tot	
BC	3159	2521	0	2521	1769	0	1819	0	1819	1529	271	1800	1400
CS1	2653	1591	1460	3051	824	1043	1864	413	2276	724	2579	3303	1994
CS2	3165	2517	0	2517	1768	0	1834	0	1834	1517	283	1800	1400
CS3	2665	1579	1460	3039	820	1046	1871	422	2294	715	2591	3306	2008
CS4	3159	2521	0	2521	1769	0	1820	0	1820	1529	271	1800	1400
CS5	3134	2538	0	2538	1771	0	1763	0	1763	1567	233	1800	1400
CS6	3134	2538	0	2538	1771	0	1765	0	1765	1567	233	1800	1400
CS7	2621	1620	1460	3080	821	1052	1842	398	2240	744	2571	3315	1973

6.5 The marginal value for ancillary services and flexible assets

The median quantities at each time interval of the marginal value of (a) PR in GB, (b) HR in GB and (c) PR in IR are shown in Fig. 9a-c. Thanks to the QP formulation of the proposed SCUC, these quantities can be easily obtained by retrieving the Lagrange multipliers of associated constraints. In particular, for all the relevant t, $max\left[\lambda_{(15a),t}, \lambda_{(15b),t}\right]$ is considered for PR in GB and IR, accordingly. However, (15a) is never binding in both areas. Similarly, $max\left[\lambda_{(32a),t}, \lambda_{(32b),t}\right]$ is adopted for HR in GB (with (32a) never binding).

Hence, in GB, the marginal value for PR is higher than the HR one, confirming the effectiveness of allocating more PR than HR to TCLs (see Fig. 8b and Table 7). Moreover, the patterns of the daily profiles are similar, i.e., higher quantity during typical low-NI conditions (night hours) and lower elsewhere. Focusing on Fig. 9a, the flexibility introduced by higher HVDC capacities (CS6, black solid line) does not produce remarkable reductions, as well as concerning CS2 where the TCL flexibility is enabled only in IR and thus is not affecting the marginal value of PR in GB.

These results represent the basis to justify a review of the current tender for fast ancillary services and the resulting prices. In fact, due to the future reduction in NI to accommodate RES, the *technical* needs of the system should be more accurately translated into *economic/financial* metrics. For example, bringing the *market value* of ancillary services closer to their *economic value* would send the better signals to stimulate investments in flexibility sources.

Similar considerations and trends discussed so far concerning the marginal value of PR in GB can be extended to the context of HR in GB and PR in IR.

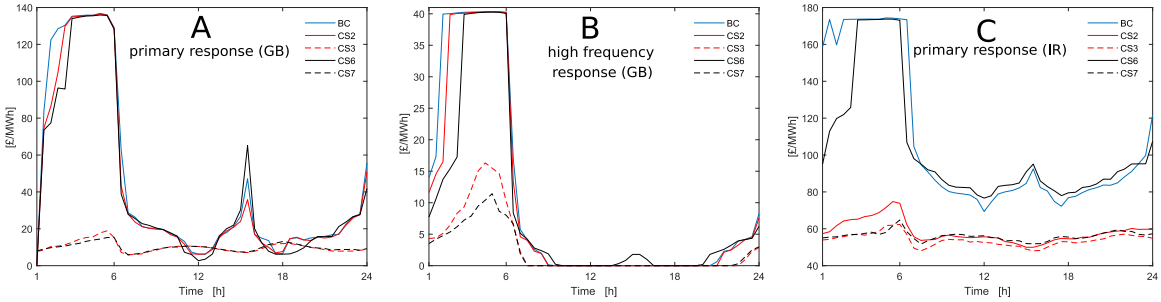

Fig. 9. Marginal value of (a) PR, (b) HR in GB and (c) PR in IR.

Finally, the half-hourly median quantities of the marginal value in increasing $\overline{I}_{CE}^{GB}$ by one unit are plotted in Fig. 10a. These quantities correspond to the Lagrange multipliers $\lambda_{(19),t}$. Case studies characterised by high total costs (i.e., BC and CS6) and that do not enable TCL flexibility exhibit high marginal values during the night hours, since the only possible (and less cost-effective, see Fig. 5a) action is to bring on line conventional generation in GB and transfer the energy, in excess of the local load, through the CE-GB HVDC. The TCL flexible operation drastically reduces the need for exporting energy (Fig. 6a and Fig. 7a), thus reducing the marginal values of the corresponding interconnector. Note that, in CS7, the rated capacity of the CE-GB HVDC link is higher than in CS3. The flection of the marginal value during the night hours up to almost zero may suggest that any additional increase in rated capacity may not be cost-effective.

Note that the marginal savings corresponding to a unitary increase in the GB-IR HVDC capacity are very often nil (median quantities equal to zero). For this reason, they have not been plotted. This result is in line with Fig. 7b, which showed low utilisation indices, implying that the interconnector is very rarely congested (i.e., keeping the associated Lagrange multipliers to zero).

On the other hand, Fig. 10b focuses on CS3 only and shows the marginal savings for the system in increasing by one unit $\overline{E}_{\mathrm{GB}}$ (red curves) and $\overline{E}_{\mathrm{IR}}$ (red curves). Once again, these quantitates correspond to the Lagrange multipliers of the right hand-side of (20) for the two areas. The median measures of these quantities are in solid lines, the mean measures in dashed lines. In general, these numerical quantities are quite low and are non-zero only in few time-intervals, indicating that TCLs are rarely constrained by thermal energy issues (as already expected by seeing Fig. 8c). For the sake of completeness, the median quantities of the Lagrange multipliers associated to the left-hand side of (20) are nil, meaning that the marginal value in decreasing the TCL thermal energy limit (i.e., letting them to reach higher temperatures) would be limited. Finally, it is worth pointing out that the marginal value, for instance of PR or HR, in each area (Fig. 9) also correspond to the Lagrange multipliers of the relevant constraints associated to TCLs.

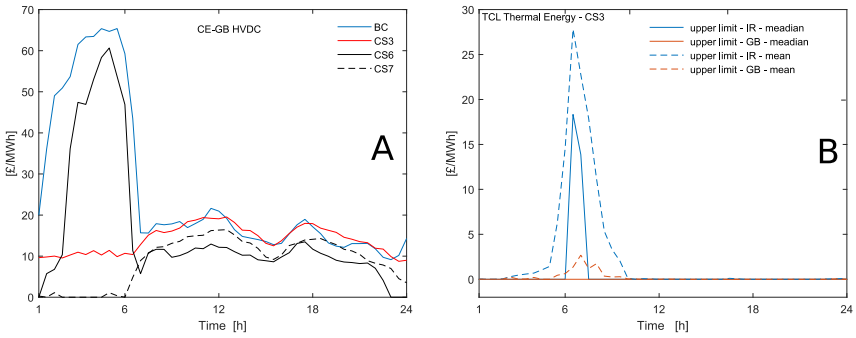

Fig. 10. Marginal value in a unitary increase of (a) the CE-GB HVDC rated capacity, (b) the TCL thermal energy in GB and IR.

7. Conclusions

This paper has introduced a novel QP formulation of SCUC for a multi-area HVDC-connected power system. The proposed model has been adopted to analyse the importance of different layers of flexibility provided by TCLs and HVDC link, accurately accounting for their intrinsic characteristics and interplay. A comprehensive set of ancillary services has been modelled to tackle all the relevant technical needs of this interconnected system.

Several case studies have been compared to a base case where TCLs are treated as inflexible load and the available HVDC capacity reflects current levels (to be reached in the near future). Case studies enable TCL flexibility in one area only, or in all the areas simultaneously, and/or increase in HVDC capacity.

Simulations have been run for different scenarios in terms of wind and load availability in different areas and import/export cost concerning the CE-GB HVDC interconnector.

The findings of this paper suggest that a critical review of the operation of future low-carbon HVDC-interconnected systems is needed. In particular, it is possible to highlight two leading factors. First, system operators or, in case of merchant assets, owners of HVDC interconnectors should no longer base feasibility studies on the benefit for interconnection only on the inter-areas energy price differentials and neglect considerations on local post-fault frequency dynamics.

Second, fundamental changes to the mechanisms that price ancillary services are necessary. In fact, this work shows how the economic value for fast ancillary services largely exceeds its market value. If proper changes are not implemented, prospective flexible assets (e.g., HVDC links) may not receive the correct market signals. This in turn may not steer the implementation of necessary technology step-ups towards the allocation of HVDC capacity based on more complex frameworks (e.g., energy and frequency response services).

In fact, the results demonstrate that the GB-IR interconnector, linking two areas largely constrained by issues related to the reduction in NI, is often operated part-loaded, with associated power flows taking directions opposite to those suggested by production cost differentials. Similar results can be extended to the operation of the CE-GB interconnector. Despite energy costs in CE are lower than those in GB, the power flows from GB to CE during those hours are characterised by low NI (high wind and low system demand).

Ongoing and future work deals with the extension of this work to a larger network to include AC cross-border interconnectors. Moreover, in the context of HVDC link, modelling advancement will be needed to

formally spare a headroom for frequency response from the interconnectors' capacity. This way the HVDC operation will have more degrees of flexibility. Moreover, as this paper focuses on the benefits of TCL and HVDC flexible operation, additional work is required to develop a detailed business model that is able to account for this value in a market-based framework. Aggregate TCLs and HVDC links would then become self-interested agents.

This paper did not aim to propose a novel market design. Therefore, the assessment of the TCL and HVDC flexibility under alternative market designs will be a relevant part of our future work.

References

[1] G.S. Seck, V. Krakowski, E. Assoumou, N. Maïzi, and V. Mazauric, "Embedding power system's reliability within a long-term energy system optimization model: linking high renewable energy integration and futuregrid stability for France by 2050," *Applied Energy,* vol. 257, p. art. 114037, 2020.

[2] S.C. Johnson, J.D. Rhodes, and M.E. Webber, "Understanding the impact of non-synchronous wind and solar generation ongrid stability and identifying mitigation pathways," *Applied Energy,* vol. 262, p. art. 114492, 2020.

[3] E. Hillberg et al., "Flexibility needs in the future power system," 2019. [Online]. Available: http://www.iea-isgan.org/wp-content/uploads/2019/03/ISGAN_DiscussionPaper_Flexibility_Needs_In_Future_Power_Systems_2019.pdf. [Accessed 10 April 2020].

[4] T.K. Chau, S.S. Yu, and T. Fernando, "A Novel Control Strategy of DFIG Wind Turbines in Complex Power Systems for Enhancement of Primary Frequency Response and LFOD," *IEEE Trans. Power Syst,* vol. 33, no. 2, pp. 1811-1823, 2018.

[5] European Commission, "Electricity interconnections with neighbouring countries - Second report of the Commission Expert Group on electricity," 2018. [Online]. Available: https://ec.europa.eu/energy/sites/ener/files/documents/2nd_report_ic_with_neighbouring_countries_b5.pdf. [Accessed 10 April 2020].

[6] National Grid, "Future Energy Scenarios," 2019. [Online]. Available: https://www.nationalgrideso.com/future-energy/future-energy-scenarios-fes. [Accessed 10 April 2020].

[7] A. Ulbig, T. Borsche, and G. Andersson, "Impact of Low Rotational Inertia on Power System Stability and Operation," *IFAC Proceedings Volumes,* vol. 47, no. 3, pp. 7290-7297, 2014.

[8] B. Hartmann, I. Vokony, and I. Taczi, "Effects of decreasing synchronous inertia on power system dynamics—Overview of recent experiences and marketisation of services," *International Transactions on Electrical Energy Systems,* vol. 29, no. 12, pp. 1-14, 2019.

[9] C. Wei, J. Xu, S. Liao, Y. Sun, Y. Jiang, and Z. Zhang, "Coordination optimization of multiple thermostatically controlled load groups in distribution network with renewable energy," *Apllied Energy,* vol. 231, pp. 456-467, 2018.

[10] G. Castagneto Gissey et al., "The value of international electricity trading," 2019. [Online]. Available: https://www.ofgem.gov.uk/system/files/docs/2019/10/value_of_international_electricity_trading.pdf. [Accessed 10 April 2020].

[11] National Grid, "Frequency response services," [Online]. Available: https://www.nationalgrid.com/uk/electricity/balancing-services/frequency-response-services. [Accessed 10 April 2020].

[12] National Grid , "FFR Market Information Jan- 20 Table," [Online]. Available: https://www.nationalgrideso.com/balancing-services/frequency-response-services/firm-frequency-response-ffr?market-information.

[13] Carbon Trust - Imperial College London, "An analysis of electricity system flexibility for Great Britain," 2016. [Online]. Available: https://assets.publishing.service.gov.uk/government/uploads/system/uploads/attachment_data/file/568982/An_analysis_of_electricity_flexibility_for_Great_Britain.pdf.

[14] J. Armatys, P. Askham, and M. Green, Principles of Valuation, Routledge, 2009.

[15] A. Tosatto, T. Weckesser, and S. Chatzivasileiadis, "Market Integration of HVDC Lines: Internalizing HVDC Losses in Market Clearing," *IEEE Trans. Power Syst.,* vol. 35, no. 1, pp. 451-461, 2020.

[16] E. Pean, M. Pirouti, and M. Qadrdan, "Role of the GB-France electricity interconnectors in integration of variable renewable generation," *Renewable Energy,* vol. 99, pp. 307-314, 2016.

[17] A. Lotfjou, M. Shahidehpour, Y. Fu, and Z. Li, "Security-Constrained Unit Commitment With AC/DC Transmission Systems," *IEEE Trans. Power Syst.,* vol. 25, no. 1, pp. 531-542, 2010.

[18] D. Van Hertem and M. Ghandhari, "Multi-terminal VSC HVDC for the European supergrid: Obstacles," *Renewable and Sustainable Energy Reviews,* vol. 14, pp. 3156-3163, 2010.

[19] Artelys Optimization Solutions, "Determination of a target electricity interconnection capacity between France and the United Kingdom," 2019. [Online]. Available: https://www.cre.fr/content/download/21153/271634%20. [Accessed 10 April 2020].

[20] POYRY, "Costs and benefits of GB Interconnection. A Poyry report to the National Infrastructure Commission," 2016. [Online]. Available: https://www.nic.org.uk/wp-content/uploads/Costs-and-benefits-of-GB-Interconnection-A-Poyry-Report.pdf.

[21] M. Aunedi, P-A. Kountouriotis, J. E. O. Calderon, D. Angeli, and G. Strbac, "Economic and environmental benefits of dynamic demand in providing frequency regulation," *IEEE Trans. Smart Grid,* vol. 4, no. 4, p. 2036–2048, 2013.

[22] E. Karangelos and F. Bouffard, "Towards full integration of demand-side resources in joint forward energy/reserve electricity markets," *IEEE Trans. Power Syst,* vol. 27, no. 1, pp. 280-289, 2012.

[23] Y. Ding et. al, "Multi-state oeprating reserve model for aggregate thermostatically controlled loads for power system short term reliability evaluation," *Applied Energy,* vol. 241, pp. 46-58, 2019.

[24] M. Zhang et. al, "Stochastic unit commitment with air conditioning loads participating in reserve service," *IET Renewable Power Generation,* vol. 13, no. 16, pp. 2977-2985, 2019.

[25] X. Han, M. Zhou, G. Li, and K. Lee, "Stochastic Unit Commitment of Wind-Integrated Power System Considering Air-Conditioning Loads for Demand Response," *Applied Science,* vol. 7, no. 1154, pp. 1-15, 2017.

[26] K. Zeng, J. Liu, L. Le, M. Zhang, Q. Zheng, and X. Ai, "Security Constrained Unit Commitment Considering Time Shift of Air-conditioning Load for Demand Response," in *4th IGBSG COnference*, Hubei, Yi-chang - China, 2019.

[27] S. Li, W. Zhang, J. Lian, and K. Kalsi, "Market-Based Coordination of Thermostatically Controlled Loads—Part I: A Mechanism Design Formulation," *IEEE Trans. Power Syst.,* vol. 2, no. 1170-1178, p. 31, 2016.

[28] V. Trovato, F. Teng, and G. Strbac, "Role and Benefits of Flexible Thermostatically Controlled Loads in Future Low-Carbon Systems," *IEEE Trans. Smart Grid,* vol. 9, no. 5, pp. 5067 - 5079, 2018.

[29] A. De Paola, V. Trovato, D. Angeli, and G. Strbac, "A Mean Field Game Approach for Distributed Control of Thermostatic Loads Acting in Simultaneous Energy-Frequency Response Markets," *IEEE Trans. Smart Grid,* vol. 10, no. 6, pp. 5987-5999, 2019.

[30] V. Trovato, A. Bialecki, and A. Dallagi, "Unit commitment with inertia-dependent and multispeed allocation of frequency response services," *IEEE Trans. Power. Syst.,* vol. 34, no. 2, pp. 1537 - 1548, 2019.

[31] K. Poncelet, E. Delarue, and W. D'haeseleer, "Unit commitment constraints in long-term planning models: Relevance, pitfalls and the role of assumptions on flexibility," *Applied Energy,* vol. 258, p. art. 113843, 2020.

[32] S. Boyd and L. Vandenberghe, Convex Optimization, New York: Cambridge University Press, 2004.

[33] L. Zhang, T. Capuder, and P. Mancarella, "Unified unit commitment formulation and fast multi-service lp model for flexibility evaluation in sustainable power systems," *IEEE Trans. Sustain. Energy,* vol. 7, no. 2, p. 658–671, 2016.

[34] T. Greve, F. Teng, M. Pollitt, and G. Strbac, "A system operator's utility function for the frequency response market," *Applied Energy,* vol. 231, pp. 562-569, 2018.

[35] Eirgrid, "Transmission system security and planning standards," 2016. [Online]. Available: http://www.eirgridgroup.com/site-files/library/EirGrid/EirGrid-Transmission-System-Security-and-Planning-Standards-TSSPS-Final-May-2016-APPROVED.pdf. [Accessed 10 April 2020].

[36] H. Holttinen et al., "Methodologies to Determine Operating Reserves Due to Increased Wind Power," *IEEE Trans. Sustain. Energy,* vol. 3, no. 4, pp. 713-723, 2012.

[37] V. Trovato, S. Tindemans, and G. Strbac, "Leaky storage model for optimal multi-service allocation of thermostatic loads," *IET Generation, Transmission & Distribution,* vol. 10, no. 3, pp. 585-593, 2016.

[38] Ofgem, "Electricity interconnectors," [Online]. Available: https://www.ofgem.gov.uk/electricity/transmission-networks/electricity-interconnectors. [Accessed 10 April 2020].

[39] D. Van Hertem, O. Gomis-Bellmunt and J. Liang, HVDC Grids for Offshore and Supergrid of the Future, IEEE Press, 2016.

[40] National Grid, "Interconnectors - Investor Relations," 2016. [Online]. Available: https://investors.nationalgrid.com/~/media/Files/N/National-Grid-IR-V2/factsheets/2016/interconnectors-factsheet-final.pdf. [Accessed 10 April 2020].

[41] A. Junyent-Ferr, Y. Pipelzadeh, and T. C. Green, "Blending HVDC-Link Energy Storage and Offshore Wind Turbine Inertia for Fast Frequency Response," *IEEE Transactions on Sustainable Energy,* vol. 6, no. 3, pp. 1059-1066, 2015.

[42] I.M. Sanz, P.D. Judge, C.E. Spallarossa, B. Chaudhuri, and T. C. Green, ""Dynamic Overload Capability of VSC HVDC Interconnections for Frequency Support," *IEEE Transactions on Energy Conversion,* vol. 32, no. 4, pp. 1544-1553, 2017.

[43] P. Tielens and D. Van Hertem, "The relevance of inertia in power systems," *Renewable and Sustainable Energy Reviews,* vol. 55, pp. 999-1009, 2016.

[44] Y. Rebours, D. Kirshen, M. Trotignon, and S. Rossignol, "A Survey of Frequency and Voltage Control Ancillary Services—Part I: Technical Features," *IEEE Trans. Power Syst.,* vol. 22, no. 1, pp. 350-357, 2007.

[45] P. Kundur, Power system stability and control, McGraw-Hill, 1994.

[46] I. A. Sajjad, G. Chicco, and R. Napoli, "Probabilistic generation of time-coupled aggregate residential demand patterns," *IET Generation, Transmission & Distribution,* vol. 9, no. 9, pp. 789-797, 2015.

[47] H. Chen, M. Liu, Y. Cheng, and S. Lin, "Modeling of Unit Commitment With AC Power Flow Constraints Through Semi-Continuous Variables," *IEEE Access,* vol. 7, pp. 52015-52023, 2019.

[48] Eirgrid, "All-Island Generation Capacity Statement 2019-2028," 2019. [Online]. Available: http://www.soni.ltd.uk/media/documents/EirGrid-Group-All-Island-Generation-Capacity-Statement-2019-2028.pdf. [Accessed 10 April 2020].

[49] M. Joos and I. Staffel, "Short-term integration costs of variable renewable energy: Wind curtailment and balancing in Britain and Germany," *Renewable and Sustainable Energy Reviews,* vol. 86, pp. 45-65, 2018.

[50] J. O'Sullivan, A. Rogers, D. Flynn, P. Smith, A. Mullane, and M. O'Malley, "Studying the Maximum Instantaneous Non-Synchronous Generation in an Island System—Frequency Stability Challenges in Ireland," *EEE Trans. on Power Syst.,* vol. 29, no. 6, pp. 2943-2951, 2014.

[51] P. Härtel et al., "Review of investment model cost parameters for VSC HVDCtransmission infrastructure," *Electric Power Systems Research,* vol. 151, pp. 419-431, 2017.

[52] Poyry, "Near-term interconnection cost-benefit analysis: independent report (cap & floor window 2)," 2017. [Online]. Available: https://www.ofgem.gov.uk/system/files/docs/2018/01/near-term_interconnector_cost_and_benefit_analysis_-_independent_report_.pdf. [Accessed 10 April 2020].

[53] ENTSO-E, "Electricity in Europe 2016," [Online]. Available: https://docstore.entsoe.eu/Documents/Publications/Statistics/electricity_in_europe/entsoe_electricity_in_europe_2016_web.pdf. [Accessed 10 April 2020].

[54] EirGrid, "DS3 System Services: Portfolio Capability Analysis," 2014. [Online]. Available: http://www.eirgrid.ie/site-files/library/EirGrid/DS3-System-Services-Portfolio-Capability-Analysis.pdf. [Accessed 10 April 2020].

[55] A. Khan, R. A. Verzijlbergh, O. Sakinci, and L. J. De Vries, "How do demand response and electrical energy storage affect (the need for)a capacity market?," *Applied Energy,* vol. 214, pp. 39-62, 2018.

[56] M. Taljegard, L. Göransson, M. Odenberger, and F. Johnsson, "Impacts of electric vehicles on the electricity generation portfolio – A Scandinavian-German case study," *Applied Energy,* vol. 235, pp. 1637-1650, 2019.